PART TWO

INFLUENCE OF STRUCTURAL FEATURES ON ZEOLITE CHARACTERIZATION BY CONSTRAINT INDEX TESTING

CHAPTER SEVEN

CONSTRAINT INDEX TESTING OF ZEOLITES

7.1 Constraint Index Test

Zeolites are microporous, aluminosilicate materials with a defined three-dimensional framework and uniformly sized pores. These materials have been used in a wide array of fields such as laundry detergents, oil and petrochemical industry, adsorbents, catalysis, separations, and agriculture.[1] The amount of research into zeolites can be demonstrated by a simple search for the term zeolite in SciFinder Scholar — this will return over 4,000 publications for each year in the current decade. These structures are both naturally occurring and synthetically produced. There are currently 191 registered structures for zeolites, of which 15 have been added in the last two years [2].

As the library of zeolite and zeolitic materials has expanded over the years, many techniques to determine both structure and shape-selectivity of these materials have been developed. One of the first described was the Constraint Index (CI) test.[3] The CI test is based on the competitive cracking of 3-methylpentane and n-hexane. The CI is calculated by Equation 1.(*X* denotes the fractional conversion of each reactant.)

$$\mathrm{CI} = \frac{\log(1 - X_{\text{n-hexane}})}{\log(1 - X_{\text{3-methylpentane}})} \qquad \textbf{(1)}$$

Thus, it is proportional to the observed cracking rate constants of n-hexane to 3-methylpentane.

In describing the CI test, Frillette and colleagues were looking for an easy test to probe the shape selectivity of new materials and to gain insights into the pore structure of those materials. From Equation 1, it can be seen that the more selective a material is for cracking n-hexane the higher the CI for that material. On the basis of CI, Frillette classified materials with a CI greater than 12 as small pore, that is, having ≤ 8 - ring pores; CI less than 1 are defined as large pore, with ≥12 - ring pores; and materials with CI between 1 and 12 as intermediate pores, having 10 - ring pores.[3] Table 7.1 lists various zeolites and their CI values, depicting the different classifications.

Since the introduction of the CI test multiple other catalytic tests have been used to probe the shape selectivity and structure of zeolites from Modified Constraint Index[4], the Spaciousness Index [5], the Shape Selectivity Index with m-xylene isomerisation [6], the alkylation of meta-diisopropylbenzene [7], and the conversion of methanol to larger hydrocarbons [8] as examples. However even with all of these tests, the CI test is the one used as a key characterization in many patents for new materials and for choosing materials in patents for new processes. Similarly it is used to help determine the unknown structures of novel materials, such as in the case of IM-5 and SSZ-57.[9] With the use of the CI test it is important that it be correct and understood why materials may deviate from the trends so that researchers are not lead to incorrect conclusions on the basis of the test. Catalytic tests are only one technique and provide a piece of information to the puzzle for understanding structures, but they can sometimes be ambiguous.

For example, the decane test reaction suggested the structure of MCM-22 had both 10 -ring and 12 -ring pores that later were determined to both be 10-ring pores.[10] There have been several structures whose CI results deviate from the classifications defined. In the earlier study by Zones and Harris it had been shown that some zeolites with known portal sizes have CI results inconsistent with the structures [11] and had shown catalytic selectivities of larger pore materials. As has been mentioned before, SSZ-35 seemed to show this anomalous behavior with Constraint Index selectivities favoring the reaction of the larger 3-methylpentane, even though the portal for the structure is closer to 5.6Å [12], not much larger than ZSM-5. Similarly SSZ-28 also falls outside the expected range based on the 8-ring pores in the structure (Figure 7.1).

7.2 Structures Containing Internal Cages

In a number of the materials in the Zones/Harris study, where there were deviations from expectations, it appeared that the structures, once known, had portals that opened into larger cages. This is not so surprising, in retrospect, as a number of new high silica zeolites have been discovered with the use of rigid polycyclic quaternary ammonium guest molecules. A recent review surveys some of this chemistry and shows the molecular modeling to illustrate the favorable energetics in locating a close host wall structure around the organo-cation guest [13]. Indeed, in terms of the details of the favorable energetics of fit, Burton et al. have recently shown interesting cage-structure selectivity for the formation of zeolite SSZ-73 [14] over another zeolite cage-structure with the use of one of two isomeric configurations for the guest molecule [15].

In this study we focus on some of these types of materials and while there is a central cage feature for locating the guest organo-cation, the consequences (if we can look at the nucleation and crystal chemistry this way for a moment) are that some pores are created as part of the unit cell. In SSZ-35 there are 10-ring portals that connect the large, shallow, 18-ring cages. Likewise SSZ-25, once calcined, has 12-ring cages that are accessed by 10-ring portals. Figure 7.2 depicts these structures with their 10-ring pores opening into larger cages. SSZ-23 with a very unusual structure of 9 and 7-rings is still a zeolite with a cage large enough to accommodate the N,N,N-1-trimethyl adamantammonium cation [16]. SSZ-28, with the DDR structure, has 8-ring portals but they traverse through larger cages formed in surrounding the bicyclic Structure Directing Agent (SDA) used in the synthesis[13]. Figure 7.3 shows the 4 different SDA used in synthesizing the cage-based zeolites in this study.

If one is crystallizing zeolites with the SDA at the center of a cage, it is natural to ask whether the external surface, at the point of terminating the crystallization, is actually not covered by “completed” cages but possibly fragments of cages. Part of the goal on the present study is to determine if such open cages exist after thermal removal of the SDA guest. And do these cages lead to non-selective surface-cracking reactions that belay the shape-selectivity that might have otherwise been observed from the pore system alone? This question had to be asked, in light of the unusual behavior of SSZ-25, whose catalytic selectivities were difficult to understand, before a structure solution came forth for the **MWW** topology [17]. In this material there appeared to be large pore zeolite selectivity that switched to intermediate pore behavior over time. We describe that, once again, in our Constraint Index studies here. Later it came to be appreciated that the material had, in essence, at least 3 types of sites for catalysis [18]. There is a hindered 10-ring which runs through the layers of the material. Cross-linking the layers leads to the creation of large cages bounded by 10-rings (larger than those within the layers). But either an incomplete cross-linking or the purposeful attempt to expose the “half-cavities” at the surface of the layers leads to a third site. While one might expect there to be less, or no shape-selectivity for these “cups” on the surface, the work of Corma on studying the selectivity for benzene alkylation — once the layered had been moved apart (ITQ-2 material) — showed shape-selectivity was nonetheless maintained [19]. So a component of our study here was to remove such exposed surface sites in all materials and answer the question as to how shape-selective behavior is affected.

7.3 Zeolite Catalyzed Hydrocabon Cracking

The Constraint Index test is based on an observed relationship of the apparent cracking rate of 3-methylpentane and n-hexane in a competitive reaction. While this study focuses on the CI test, and as such the apparent cracking rates observed on the various zeolites, one should be mindful of the multiple aspects that go into the observed cracking of hydrocarbons over acid sites on zeolite structures. Understanding the aspects of cracking from reactant adsorption to reaction mechanism to product desorption has been the focus of much work.[20 – 28] In hydrocarbon cracking, the branched isomer has a higher intrinsic reactivity than the linear isomer.[3] Any CI greater than 1 would represent a selective influence of the zeolite on the reaction.

One method by which a zeolite can impose shape selectivity on a reaction is through reactant selectivity excluding large reactants while smaller reactants can enter the structure [27] or through significant differences in diffusion into and through the structure. Work on ZSM-5 has shown the cracking rate of n-hexane and 3-methylpentane was insensitive to crystal size [3, 28] and the diffusivities of the two reactants were similar [28]. Since the cracking rates of both reactants were not affected by crystal size on ZSM-5, medium and large pore zeolites do not impose significant transport limitations or large differences in reactant diffusivities in the CI test; however, for smaller pore zeolites the influence of reactant selectivity and reactant diffusivities must be considered.

Another form of shape selectivity a structure can provide is a transition-state selectivity in which the structure has an effect on the transition states of the reaction mechanism by either sterically hindering the transition state [27] or by effects on entropy and enthalpy factors [26]. Catalytic cracking of alkanes has been shown to proceed through two mechanisms, either monomolecular cracking or bimolecular cracking [20 – 26]. In the monomolecular mechanism, a single reactant molecule undergoes a C-C bond cleavage on an acid site and desorbs to create an olefin and paraffin and regenerate the acid site. [23] In the bimolecular pathway, a carbenium ion left on the site reacts with another reactant molecule to form cracking products and leave a carbenium ion on the surface. [23] It has also been suggested that the intermediate is a covalent alkoxide species. [21] In either case, a transition-state is required for these mechanisms. The biomolecular mechanism would be more susceptible to steric restrictions as more space is needed for a reactant molecule to interact with a surface species. The biomolecular mechanism is favored at lower temperatures and higher surface concentrations of alkanes.[20] The increasing contribution of the monomolecular mechanism with increasing temperature has been credited with the decrease in CI value with increasing temperature observed on ZSM-5. [3] Several studies have shown how structural effects on hydrocarbon conversions over zeolites extends beyond steric restrictions.[25,29 – 32] Bokhoven showed the difference in observed activity for n-hexane monomolecular cracking over several structures arises in large part from the difference in the heat of adsorption which increases with decreasing pore size.[29] Earlier work by Lercher detailed that this relationship between increasing pore size and decreasing heat of adsorption, as well as the unhindered adsorption of singly branched alkanes, is limited to pore sizes of 0.5nm and greater.[30] In another example, Bokhoven demonstrates how the ability of geometrical and electronic environment around the active site influences the stability of alkoxide species in the dehydrogenation of propane and as such has a strong influence on the observed activity, as the rate-limiting step is the desorption of that species.[31] In a similar observation of structural effects on transition states, Iglesia expounds upon the cracking of propane and n-butane in the 8-member ring side pockets of H-MOR and explains the entropy gains from the partial transition confinement in the side pockets that lead to a decrease in the transition state free energy.[26] Zeolites containing cages can demonstrate transition-state selectivity that differs from other structures with similar sized pore windows by having less steric hindrance in the cage or almost no steric hindrance in external surface features.

Work by Corma [24] and van Santen [22] have shown the determination of cracking mechanism for hexane cracking is very difficult if at all possible and open to different interpretations based on reaction results alone, since the complex set of possible secondary and side reactions can lead to similar results for multiple schemes. Based on the work of Corma [22] and van Santen [24], this study has not attempted to quantify the contributions of each reaction mechanism on the CI test. Instead the conditions for the CI test on the medium and large pore zeolites are performed at conditions (i.e., low temperature, 330°C, and high hydrocarbon partial pressure, 35 kPa) that strongly favor bimolecular cracking. These conditions are similar, including contact time, to those shown by Lunsford [20] and are predominately bimolecular cracking for BEA* and ZSM-5 (and — due to the similar pore window size and large internal cages — should also be bimolecular for SSZ-25 and SSZ-35). The temperature in the CI test on the smaller pore zeolites had to be raised to achieve reasonable conversions and thus may have increased influence from the monomolecular mechanism on the results.

7.4 **References**

[1] T. Maesen, B. Marcus, in H.V. Bekkum, E.M. Flaningen, P.A. Jacobs (eds) Studies in surface Science and Catalysis 137, Elsevier Science, 2001, p.1

[2] IZA Structure Commission, *Framework Type Codes*, accessed 4/15/2009 at www.iza-structure.org

[3] V.J. Frillette, W.O. Haag, R.M. Lago, J. Catal. 67 (1981) 218.

[4] J.A. Martens, M. Tielen, P.A. Jacobs, J. Weitkamp, Zeolites 4 (1984) 98.

[5] J. Weitkamp, S. Ernst, R. Kumar, Appl. Catal. 27 (1986) 207.

[6] F. Joensen, N. Blom, N.J. Tapp, E.G. Derouane, C. Fernandez, Stud. Surf. Sci. Catal., 49(A) (1989) 1131.

[7] M.H. Kim, C.Y. Chen, M.E. Davis, ACS Symp. Ser. 1993, 517, 222.

[8] L-T Yuen, S.I. Zones, T.V. Harris, E.J. Gallegos, A. Auroux, Microporous Mater. 2 (1994) 105.

[9] S.I. Zones, C.Y. Chen, A. Corma, M.T. Cheng, C.L. Kibby, I.Y. Chan, A.W. Burton, J. Catal. 250 (2007) 41.

[10] W. Souverijns, W. Verreist, G. Vanbutsele, J.A. Martens, P.A. Jacobs, J. Chem. Soc., Chem. Commun., 14 (1994) 1671.

[11] S.I. Zones, T.V. Harris, Micro. Meso. Mater. 31 (2000) 35.

[12] P. Wagner, Y. Nakagawa, G.S. Lee, M.E. Davis, S. Elomari, R.C. Medrud, S.I. Zones, J. Am. Chem. Soc. 122 (2000) 263.

[13] A.W. Burton, G.S. Lee, S.I. Zones, Micro. Meso. Mat. 90 (2006) 129.

[14] D.S. Wragg, R.E. Morris, A.W. Burton, S.I. Zones, K.K. Ong, G.S. Lee, Chem. Mat. 19 (2007) 3924.

[15] C. Kim, S-J. Hwang, A.W. Burton, S.I. Zones, Micro. Meso. Mat. 116 (2008) 227.

[16] M.A. Camblor, M.J. Diaz-Cabanas, J. Perez-Pariente, S.J. Teat, W.W. Clegg, I.J. Shannon, P. Lightfoot, P.A. Wright, R.E. Morris, Angew. Chem. Intl. Ed. 37 (1998) 2122.

[17] M.E. Leonowicz, J.A. Lawton, S.L. Lawton, M.K. Rubin, Science, 264, (1994) 1910.

[18] P. Matias, J.M. Lopes, S. Laforge, P. Magnoux, M. Guisnet, F.R. Ribeiro, Appl. Catal. A: Gen. 351 (2008) 174.

[19] A. Corma, V. Fornes, S.B. Pergher, Th.L.M. Maesen, J.G. Buglass, Nature 396 (1998) 353.

[20] S. Kotrel, M.P. Rosynek, J.H. Lunsford, J. Phys. Chem. B 103 (1999) 818.

[21] A.M. Rigby, G.J. Kramer, R.A. Van Santen, J. Catal. 170 (1997) 1.

[22] M.V. Frash, R.A. Van Santen, Topics Catal. 9 (1999) 191.

[23] A. Corma, A.V. Orchilles, Micro. Meso. Mat. 35-36 (2000) 21.

[24] A. Corma, P.J. Miguel, A.V. Orchilles, J. Catal. 172 (1997) 355.

[25] A. Bhan, R. Gounder, J. Macht, E. Iglesia, J. Catal. 253 (2008) 221.

[26] R. Gounder, E. Iglesia, J. Amer. Chem. Soc. 131 (2009) 1958.

[27] S. Csiscery, Zeolites 4 (1984) 202.

[28] W.O. Haag, R.M. Lago, P.B. Weisz, Faraday Discuss. Chem. Soc. 72 (1981) 317.

[29] J.A. van Bokhoven, B.A. Williams, W.Ji, D.C. Koningsberger, H.H. Kung, J.T. Miller, J. Catal. 224 (2004) 50.

[30] F. Eder, J.A. Lercher, J. Phys. Chem. B 101 (1997) 1273.

[31] B. Xu, C. Sievers, S.B. Hong, R. Prins, J.A. van Bokhoven, J. Catal. 244 (2006) 163.

[32] Q.L. Wang, M. Torealba, G. Giannetto, M. Guisnet, G. Perot, M. Cahoreau, J. Caisso, Zeolites 10 (1990) 703.

Figure 7.1: Examples of two structures whose CI values fall outside expected ranges for their pore size

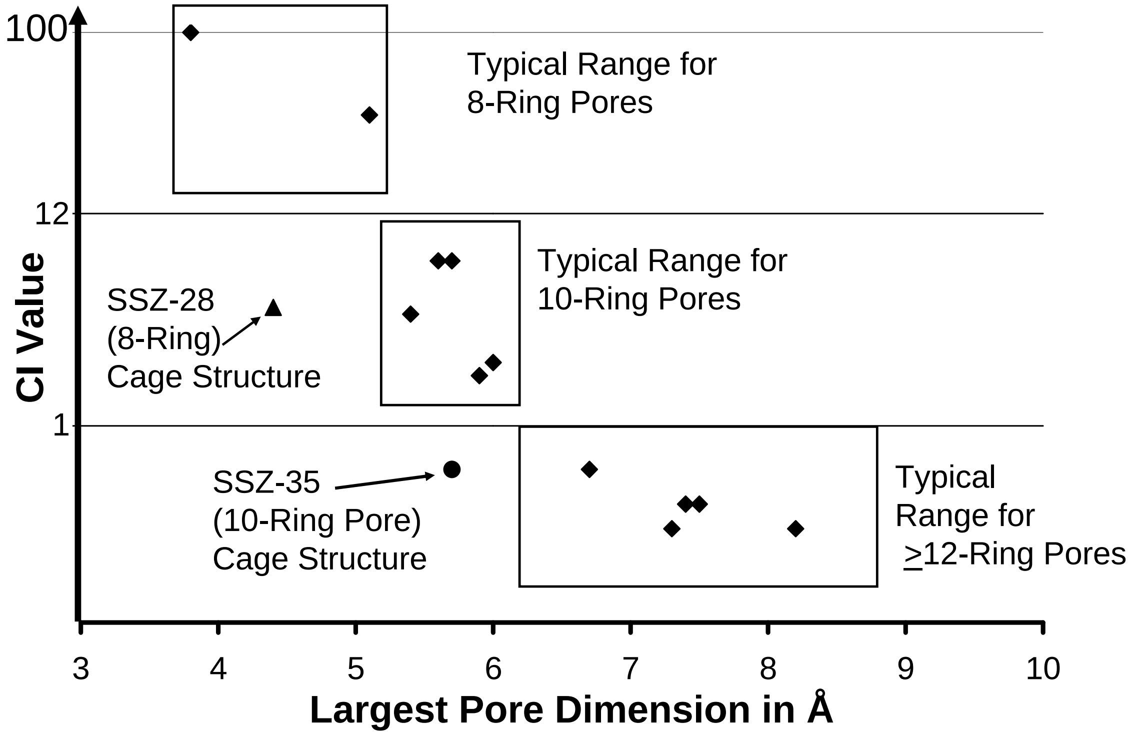

Figure 7.2: Examples of structures (a) STF, (b) STT, (c) MWW and (d) DDR with pores opening into larger cages along with (e) MFI and (f) BEA as comparisons of structures without cages

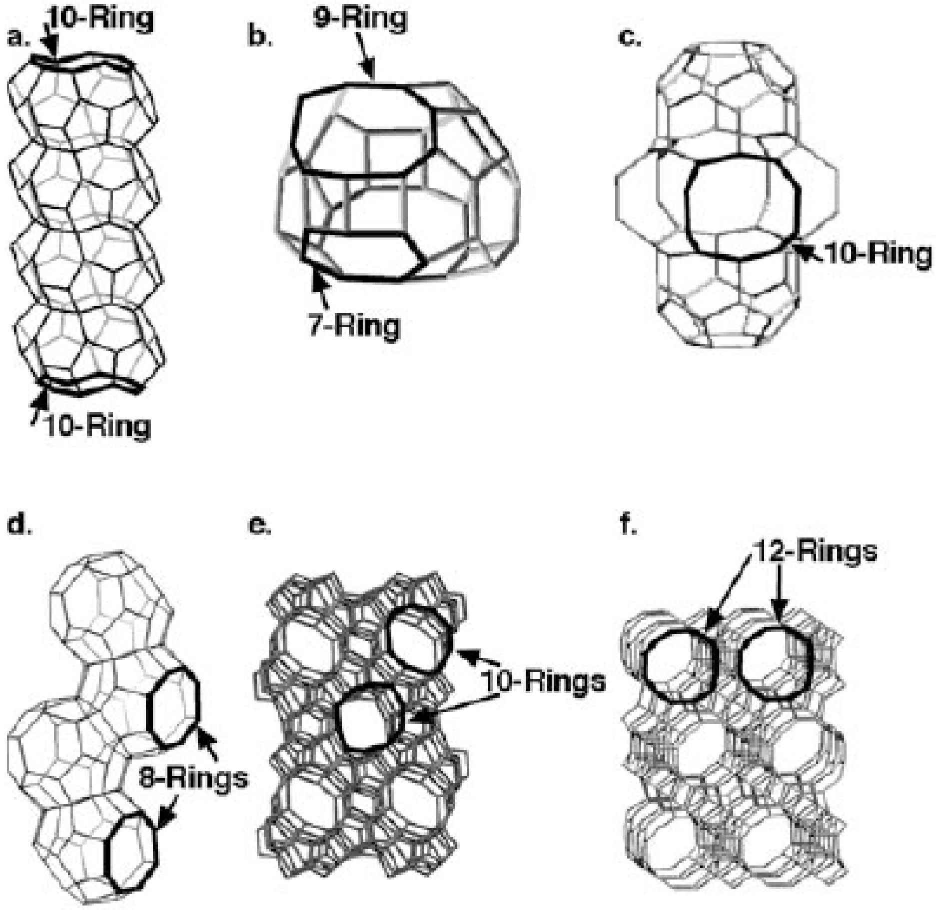

Figure 7.3: Structure Directing Agents used to make the 4 structures with cages in Figure 7.2. SSZ-35 (STF), SSZ-23 (STT), SSZ-25 (MWW) and SSZ-28 (DDR)

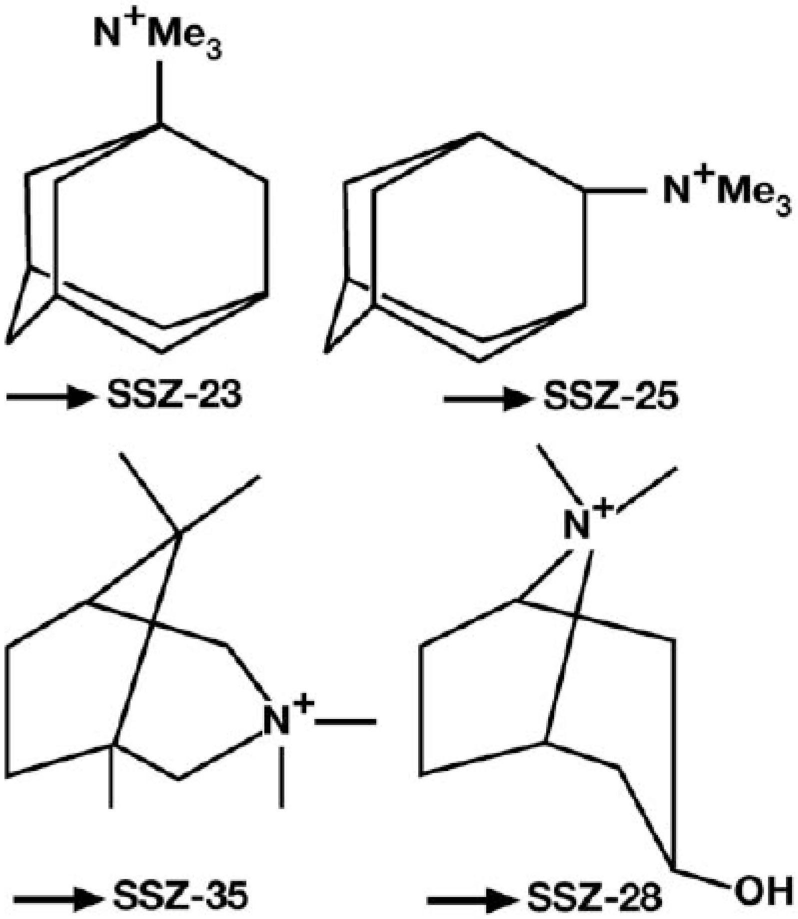

Table 7.1: Examples Constraint Index Values

Zeolite	**Pore Apertures**	**CI**
SSZ-13	8-ring	>100
Erionite	8-ring	38
ZSM-23	10-ring	10.6
SSZ-20	10-ring	6.9
ZSM-5	10-&10-ring	6.9
EU-1	10-ring	3.7
ZSM-12	12-ring	2.1
SSZ-31	12-ring	0.9
LZY-82	12-rings	0.4
CIT-5	14-ring	0.4
SSZ-24	12-ring	0.3
UTD-1	14-ring	0.3

CHAPTER EIGHT

EXPERIMENTAL METHODS FOR INVESTIGATION OF CONSTRAINT INDEX TESTING

8.1. Zeolite Synthesis

The zeolites used in the study were synthesized at Chevron by the following procedures in all cases except for the Beta zeolite. This material was obtained from the TOSOH Corporation as product number HSZ930NHA still containing the structure-directing agent. Unless specified, the BEA* sample was calcined upon receipt and 2 ion-exchanges with Ammonium nitrate (95 °C, 2 hours) were performed before use.

ZSM-5

In a 23 ml Teflon Cup for a Parr 4845 reactor the following set of reagents were combined. 0.11 grams of Reheis F-2000 alumina hydroxide gel (25% Al) was dissolved into a basic solution of 1.9 grams of 40% tetrapropylammonium hydroxide, 3.35 grams of 1 N NaOH, and 1 ml water. Once the solution was clear, 4.5 grams of Ludox AS-30 was stirred in. The reactor was closed, loaded onto a spit in a convection heated oven and tumbled while being heated at 170 ºC for 5 days. The product was collected upon cooling and verified to be ZSM-5 by XRD analysis. The product was then given a calcination to 595 ºC by a program of heating at 1ºC/min to 120 ºC (hold for 2h), at 1 ºC/min to 540 ºC (hold for 5h), and at 1 ºC/min to 595 ºC (hold for 5h) to remove the SDA. After which, 2 ion-exchanges with ammonium nitrate solution (95 ºC, 2 hours each) were performed before use in catalytic studies.

SSZ-25

The sample of SSZ-25 used in this study came from a 5 gallon preparation of the material using a mixed SDA systems of N,N,N, 2-trimethyladamantammonium hydroxide (see Fig. 7.3) and piperidine as a pore filler.[1] A similar post–crystalllization was provided except the SSZ-25 is given 4 ion-exchange treatments after the calcination.

SSZ-23

A reaction was set up as in ZSM-5 above with the following reagents and quantities. For Reheis F-2000 we dissolved 0.03 grams into a solution of 3.75 mMoles of N,N,N 1trimethyl adamantammonium hydroxide (Fig. 7.3) in 7 ml of water. An additional 4.5 ml of water with 10-4 Molar concentration of methylene blue was added in [2]. 1.2 grams of 1N KOH solution were added. Once clear, 0.90 grams of Cabosil M-5, fumed silica (~ 15 mMoles) were stirred in and the reactor was given 3% seeds of SSZ-23 [19] and heated at 160 ºC and 43 RPM for 7 days. The product work-up was similar to that for ZSM-5.

SSZ-28

In a manner similar to the ZSM-5 synthesis, the following reagents were mixed. 3.25 mMoles of N-methyl tropinium hydroxide (Fig. 7.3) in 10ml of water is given 1.5 mMoles of NaOH . Y zeolite is added as an AL source for the reaction (LZY-52 which has about 16 wt % Al2O3). 0.76 grams of Cabosil M5 was stirred in and the reaction was run at 160 ºC and 43 RPM tumbling for 6 days. The work-up of this material differs from the others. The washed crystalline solid was analyzed and found to be all SSZ-28. But as a precaution, since Y zeolite is employed in the synthesis, we degraded any remaining trace Y by heating the solids in 10ml N HCl/gm zeolite material at 95 ºC in a closed reactor for 2 days. The product was then washed and calcined and ion-exchanged as above. This process may remove any surface sites in the SSZ-28 as well, prior to our surface studies.

SSZ-35

The sample of SSZ-35 was taken from a batch made in a 1 gallon reactor run at 160 ºC, 75 RPM for a course of 16 days. The ratio of reagents was as follows: The organo-cation to SiO2 ratio was 0.10 with the reagents being the SDA from pentamethyl (1,6,6,8,8,) bicyclo[3.2.1]-6-ammonium-octane (Fig. 7.3) and Ludox AS-30 (30 % SIO2). SiO2/Al2O3 = 35 with Reheis F2000 as Al source. KOH/SiO2 = 0.20 and H2O/SiO2 = 35.

8.2. External Surface Modification

In several cases the samples' external surfaces were dealuminated following the procedure described by Breck and Skeels[3] using an aqueous ammonium hexafluorosilicate treatment. Samples were taken before calcinations to maintain the SDA inside the structure. 2g of zeolite were stirred in 50ml of an aqueous ammonium acetate solution (2M, 75 °C). Separately, 1.5g ammonium hexafluorosilicate was dissolved in 50ml of water. The ammonium hexafluorosilicate solution was added drop wise over 3 hours to the zeolite mixture once the mixture had reached 75° C. After addition of the ammonium hexafluorosilicate solution was complete the mixture was heated to 95 °C and stirred with condenser for 12 hours. The zeolite was then filtered from the mixture and washed with a minimum of 500ml hot water before air drying.

8.3 Reactivity Tests

Reactivity was tested in by both hydrocarbon cracking and isopropanol dehydration. Samples for reaction tests were prepared by pelletizing and then crushing that pellet of either the acid or NH4+-form of the zeolites. The crushed samples were sieved to collect the 20 – 40 mesh fraction. Typically 0.50g (~1ml) of sample was loaded into the reactor tube packed between glass wool. The sample was then heated to 350 °C under an argon flow of 25cm^3/min for at least 4 hours before reactions commenced.

All reactions were performed in a BTRS Jr. Reactor (Autoclave Engineers, see Figure 8.1 for reactor schematics) equipped with a ½-inch stainless steel reactor tube. The system also has a reactor bypass loop allowing equilibration of the feed stream in the system before introducing the feed to the catalyst. The hydrocarbon feeds for both tests were fed as a liquid by syringe pump into a mixing assembly where it was vaporized with a sweep gas of 5% argon in helium (AirLiquide, 99.999%) in a mixing assembly at 150 °C. The n-hexane, 3-methylpentane, and isopropanol feeds were all used as purchased form Sigma-Aldrich with purities greater than or equal to 99.9%. The helium/argon feed was controlled by a Brooks Instrument mass flow controller and the hydrocarbons by the Harvard Apparatus syringe pump. The reactor effluent was fed directly to a multi-port valve for gas sampling. The product lines from the reactor and the sample valve were heated to approximately 150^{o}C to prevent liquid condensation. The product analysis was done by GC/MS (Agilent GC 6890N/MSD 5973N) utilizing a capillary column (HP Plot Q). Samples were run at a temperature program of 150^{o}C for two minutes (to allow gas sampling) and then heating to 175^{o}C at 2.33^o/min Products were identified from the GC/MS results by both the MS results for each peak as well as retention times from injections of individual components purchased from Sigma-Aldrich (99%+ purity). The retention times were argon at 1.3 min, methane at 1.35min, ethene at 1.44 min, ethane at 1.54min, propene at 1.8min, propane at 1.87min, isobutane at 2.63, isobutene at 2.73min, n-butane at 2.93min, n-butene at 3.02, n-pentane at 5.64min, 2mehtylbutane at5.1 min, n-hexane at 9.49min and 3-methylpentane at10.3min. The results were quantified using the argon in the He/Ar sweep gas as an internal standard. Calibration curves on the basis of mols product/mols Ar vs. MS counts product/MS counts of Ar for each of the products were generated by flowing various concentrations of the known product mixtures with various sweep gas flow rates through the system in bypass mode.

Typical Constraint Index test and single reactant cracking conditions were a reaction temperature of 330 °C and atmospheric pressure with 0.5g of zeolite. The reactant liquid feed was at a LHSV of 1.67h-1. Isopropanol dehydration used a lower temperature of 150°C. For the Constraint Index test a mixture of 50mol% n-hexane and 50mol% 3-methylpentane was used. These conditions were adjusted to try and reach conversions between 10 – 60% when possible for the Constraint Index test.

8.4. Zeolite Characterization

Zeolite structures were determined and monitored powder X-ray diffraction on a Scintag XDS 2000 diffractometer. Micropore volumes of the zeolites were measured by nitrogen adsorption on a Micromeritics ASAP 2000 instrument. SEM on a LEO 1550 VP field emission scanning electron microscope was used to measure crystal size. Elemental analysis data for calculating the silicon to aluminum ratio (SAR) of the bulk material were obtained from Galbraith Analytical in Knoville, TN, utilizing inductively coupled plasma–optical emission spectroscopy (ICP-OES). A Netzsch STA 449C Jupiter system was used to record simultaneous thermogravimetric analyses (TGA) and differential scanning calorimetry (DSC). Samples were loaded into Al_2O_3 crucibles and heated to 900°C at 5 K/min under 50mL/min inert gas. The TGA/DSC measurements were utilized for measuring at what temperature SDA degradation began and the mass of carbon-species built up during cracking reactions. The measurements of surface compositions were made using a commercial XPS, an Ulvac Phi Quantera Scanning Microprobe. The particles making up the samples were like small grains of sand of dimension approximately 0.5 – 1.5 mm, and closely packed for analysis. The X-ray spot defined the analysis area, a rectangle 1.4mm x 0.1 mm, and so many analyses sampled more than one particle. The scans were made with a nominal spectral resolution of 1.05 eV. For all samples multiple analysis areas were scanned, and the tabulated data represent the determined average and standard deviation. The XPS raw signal intensities were normalized using empirical sensitivity factors by standard XPS data handling software, and compositions are given in atom-%.

8.5. n-Hexane and 3-Methylpentane Adsorption

Adsorption of n-hexane and 3-methylpentane was carried out using a Cahn C-2000 balance couple with a computer interface previously described in the literature [4]. Approximately 20mg of sample was dehydrated in vacuum at 450 °C for 1 h prior to the adsorption. The relative partial pressure P/Po of both n-hexane and 3-methylpentane was kept at ~0.3 during the adsorption of each individually. The measurements were made at room temperature.

8.6 References

[1] S.I. Zones, S.J. Hwang, M.E. Davis, Chemistry — A European Journal 7 (2001) 1990.

[2] S.I. Zones, Y. Nakagawa in: L. Bonnevoit, S. Kaliaguine (Eds.) Zeolites: A refined Tool, Elsevier, Amsterdam (1995) 45.

[3] D. Breck, G. Skeels, US patent 4 503 023 (1985) to Union Carbide Corporation.

[4] C.Y. Chen, S.I. Zones, Micro. Meso. Mat. 104 (2007) 39–45.

Figure 8.1: Flow diagram of BTRS Jr. reactor system for ispropanol dehydration and hydrocarbon cracking

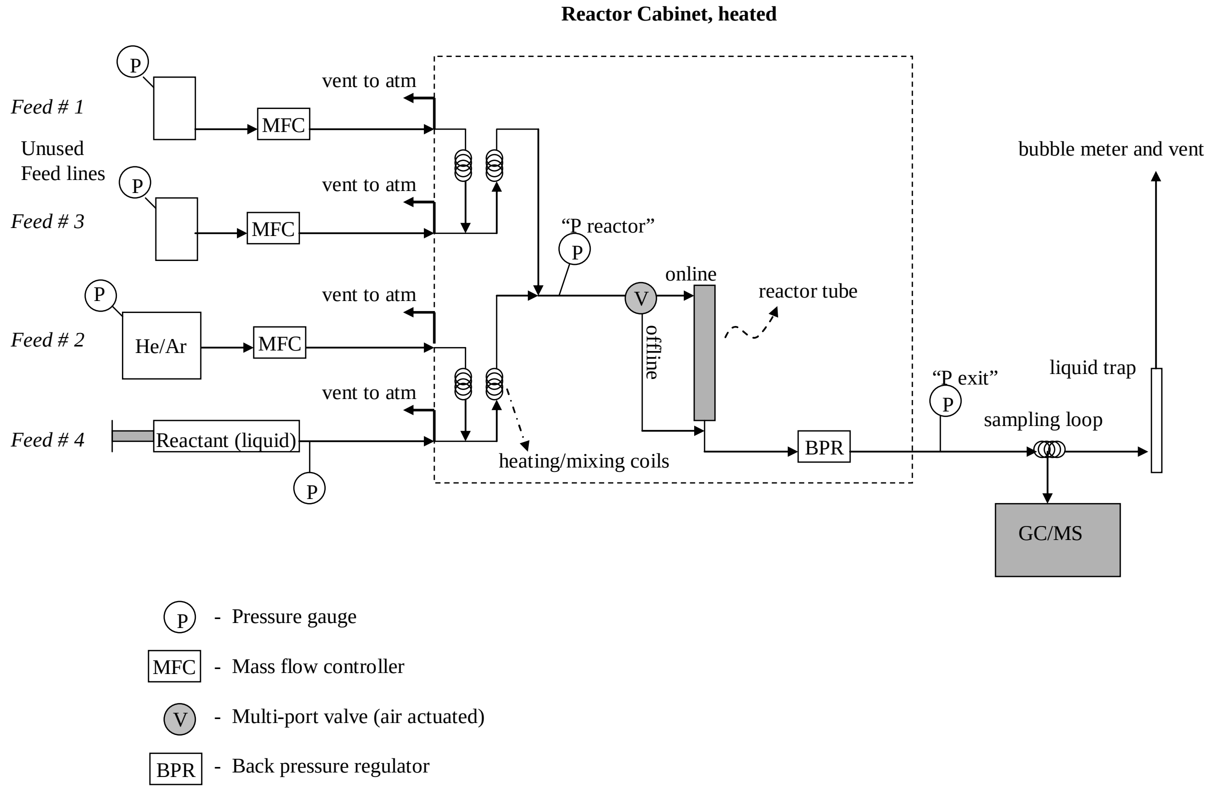

CHAPTER NINE

EFFECT OF EXTERNAL SURFACE ACTIVITY ON CONSTRAINT INDEX TESTING

When faced with reduced selectivity in a shape-selective reaction, one must consider situations that would reduce the selective influences, whether from reactant selectivity imposed by a pore size blocking large reactants, or steric constraints at the active site limiting the viable transition-states. In zeolites these shape selective limits arise from the majority of active sites being internal to the pore structure. However, sites located on the external surface would not be restricted by the structure and have less shape selective limits. In fact for small crystal zeolites, the external surface can have an important contribution to activity especially for reactions that are either very rapid or highly diffusion limited.[1] For the **MWW** structure (the structure of SSZ-25), incomplete cages have been shown to form cup-like hemicages on the external surface.[2] These cups on the surface have been shown to be active in the cracking of 1,3-diisopropylbenzene and vacuum gasoil on ITQ-2 [3] and in methylcyclohexane transformations on MCM-22 [4].

The influence of the external surface on Constraint Index characterization of structures containing large cages waas investigated in this work by passivating the external surface. Reduction in external surface activity was accomplished by removal of external active sites by dealumination. The dealumination of zeolites can be accomplished through multiple techniques, many detailed in review on the subject by Beyer.[5] Hydrothermal treatment and acid leaching result in increased defects and mesopores.[5] Isomorphous subsititiution by $SiCl_4$ must be performed at elevated temperatures around 500°C which would degrade and lead to loss of the SDA[5]. Aqueous isomorphous substitution with ammonium hexafluorosilicate, on the other hand, proceeds at temperatures near 100°C[6]. This temperature allows the SDA to remain in the pores, limiting the dealumination to the external surface if performed before calcinations. As such, ammonium hexafluorosilicate treatment was utilized to passivate the external surface. This process is shown in Figure 9.1

9.1 Characterization

Samples of ZSM-5, BEA*, SSZ-25, and SSZ-35 were dealuminated following the process of Breck and Skeels[6] except the SDA was left in the structure during the modification to block the interior pores and limit the dealumination to the external surface. Table 9.1 details the characterization of each sample in both the parent zeolite and the dealuminated samples. XPS analysis of the external surface demonstrates a larger increase in the Si/Al ratio for the external surface than the change in the bulk Si/Al. It should be noted the XPS technique samples a near surface depth (2-20nm, or the equivalent of a few unit cells [12]) into the sample thus the actual Si/Al ratio for the external surface may be higher than the XPS measurement. (See section 8.4 for XPS details.) Also the decrease in the micropore volume by the ammonium hexafluorosilicate dealumination process is expected from previous work.[7] XRD (Figure 9.2) and SEM (Figure 9.3) analysis show little change in the crystallinity and crystal size of each sample by the treatment. All samples in the study were crystals 1μm or less in size, which led to difficulty in getting good morphologies from the SEM.

9.2 Isopropanol Dehydration

Isopropanol dehydration was also used to characterize the effect of the dealumination process on the BEA*, ZSM-5, and SSZ-35 samples. The low temperatures, 170 – 180°C, needed to transform isopropanol to propene and diisopropylether[8] over acid zeolites makes this an attractive test reaction because the SDA can be maintained in the pores of the zeolite limiting the measurement to the external surface activity only. These zeolites can be activated by thermal treatment at 350 °C in a flowing stream of inert gas and still maintain their SDA inside their structure. 350 °C was found to be the lowest treatment temperature that could be used for zeolite activation to achieve the same activity of calcined materials. Figure 9.4 shows the SDA of ZSM-5, BEA*, and SSZ-35 maintained at temperatures below 350 °C. The SDA of SSZ-25 undergoes decomposition at temperatures below 350 °C (Figure 9.5) and thus was not characterized this way. Figure 9.6 shows the rate of isopropanol consumed at 15 minutes on stream and 180 °C. The dealumination process does not completely eliminate the activity of the samples to the same level of pure silicon sample of BEA*. This is probably due to the ability of the smaller isopropanol molecule to reach sites located in the pore entrances that the hexafluorosilicate could not access but is not also blocked by the SDA. However, for all samples we see a greater than 50% reduction in the rate of isopropanol consumed. The parent sample of SSZ-35 has a lower external surface activity than the BEA* sample and a lower activity than the calcined sample of SSZ-35 suggesting a small impact, if any, on the external surface of SSZ-35. While the external surface activity toward isopropanol dehydration is not completely quenched by the ammonium hexafluorosilicate treatment the large reduction would still produce an observable change in the Constraint Index test if the external surface activity is important.

9.3 Constraint Index Testing

Figure 9.7 shows the comparison of the CI Test for the calcined parent and calcined dealuminated samples. The observed behavior of BEA^* and ZSM-5 is consistent with literature reports for these structures and the dealumination process appears to only slightly reduce the activity. Similarly SSZ-35 shows only a small reduction in activity and similar CI values over time on stream. For all three samples, the dealumination process had no major effect on the CI Test. This suggests the external surface has little impact on the CI Test, and is not the reason for the CI value of SSZ-35 resembling a large pore structure, even though it is a medium pore structure. The reductions in activity likely arise from the loss of some internal sites due to pore blocking, as evident from the decrease in micropore volume detailed in Table 9.1. More evidence of the lack of surface activity for the cracking of n-hexane and 3-methylpentane can be seen on SSZ-35 where the SDA is left in the structure as a pore blocking agent and limits the activity to the external surface. The SDA of SSZ-35 blocks the pores of the structure throughout the reaction as seen by the TGA/DSC analysis as well as N2 adsorption before and after testing. When the CI Test is run on SSZ-35 still containing the SDA no cracking was observed, even at the initial time point. The external surface either deactivates by the rapid build-up of deactivating carbon species or is inactive toward cracking and with either case has no influence on the CI test, whose values are typically reported at the 10 to 20 minute time point.

SSZ-25 in Figure 9.7 does show a significant deviation in the behavior of the parent and dealuminated sample in the CI Test. The initial 45 minutes are similar. However, after that the dealuminated sample deactivates quicker and the CI value of the dealuminated sample increases at a slower rate. This change in the CI value is opposite the change expected if the external surface is having a significant effect. The external surface would be expected to have no shape selectivity and thus lower the CI value. Reducing the external surface effect by dealumination would be expected to give a higher initial CI value and quicker increase than the parent sample. As such, the external surface does not appear to be responsible for the low CI value of SSZ-25, or the increasing behavior of the CI value.

This behavior is consistent with the recent study by Guisnet for the transformation of n-heptane over MCM-22. Guisnet showed that the large initial drop in activity is from the deactivation of the large cages by coke formation with a quasi-plateau in activity remaining from the sinusoidal channels and in the cracking reaction the external cups were not active [9]. The activity pattern in Figure 9.7d for SSZ-25 follows the same deactivation behavior for the CI test as Guisnet's n-heptane cracking. The increasing CI value over time on stream could then be thought of as coming from the shift from most of the activity occurring in the large cages initially with a low CI, to most of the activity occurring at later times in the sinusoidal channels with a high CI value.

A similar indication that the behavior of SSZ-25 is not related to the surface but instead the internal structure is the shift in the $i\text{-}C_4/n\text{-}C_4$ product ratio over time. Zones and Harris [10] detailed the link between $i\text{-}C_4/n\text{-}C_4$ product ratio and the CI value where materials with higher CI values have lower $i\text{-}C_4/n\text{-}C_4$ ratios presumably due to less conversion of 3-methylpentane. It should be noted that they saw no change in the ratio on

ZSM-5 when changing temperatures and thus change the total feed conversion.[10] On both the parent sample and the surface deactivated sample of SSZ-25, the i-C_4/n-C_4 ratio is around 5 at 15 minutes on stream and decays to 2.2 by 6 hour on stream, indicating a significant reduction in the branched products over time. For zeolites ZSM-5, BEA*, and SSZ-35 the ratios are 1.1, 4.5, and 4, respectively, and remain relatively constant over 6h on stream. With an inactive surface, this change in SSZ-25's i-C_4/n-C_4 in comparison to the constant values of the other structures would result from a shift in the reaction from the cages in the structure to the more restricted sinusoidal channels. Since the pore sizes into the cages and the channels are similar and smaller than ZSM-5 [11], SSZ-25 suggest the larger internal space is responsible for the CI value rather than external surface activity or pore size.

9.4 References

[1] M. Farcasiu, T. F. Degnan, Ind. Eng. Chem. Res. (1988) 27, 45.

[2] S.L. Lawton, M.E. Leonowicz, R.D. Partridge, P. Chen, M.K. Rubin, Micro. Meso. Mater. 23 (1998) 109.

[3] A. Corma, V. Fornes, S.B. Pergher, Th.L.M. Maesen, J.G. Buglass, Nature 396 (1998) 353.

[4] P. Matias, J.M. Lopes, S. Laforge, P. Magnoux, P.A. Russo, M.M.L. Ribeiro Carrott, M. Guisnet , F. Ramoa Ribeiro, J. Catal. 259 (2008) 190.

[5] H.K. Beyer in H.G. Karge, J. Weitkamp (eds.), Molecular Sieves Science and Technology, Springer, 2002, 203.

[6] D Breck, G. Skeels, US patent 4 503 023 (1985) to Union Carbide Corporation.

[7] Q.L. Wang, M. Torealba, G. Giannetto, M. Guisnet, G. Perot, M. Cahoreau, J. Caisso, Zeolites 10 (1990) 703.

[8] S.J. Gentry, R. Rudham, J. Chem. Soc. Faraday I 70 (1974) 1685.

[9] P. Matias, J.M. Lopes, S. Laforge, P. Magnoux, M. Guisnet, F.R. Ribeiro, Appl. Catal. A: Gen. 351 (2008) 174.

[10] S.I. Zones, T.V. Harris, Micro. Meso. Mater. 31 (2000) 35.

[11] M.E. Leonowicz, J.A. Lawton, S.L. Lawton, M.K. Rubin, Science, 264, (1994) 1910.

[12] K. Klier in “ Spectroscopic studies of zeolites and mesoporous materials” in J. Cejka, H. van Bekkum (eds.) Studies in Surf. Sci. 157 (2005) Elsevier B.V., Netherlands, 205.

Figure 9.1: Ammonium hexafluorosilicate dealumination scheme

$$\mathrm{(NH4)^{+}_{x}[Al_{x}Si_{y}O_{(2x+2y)}]^{x-} + (NH_{4})_{2}[SiF_{6}]}$$

$$\Big\downarrow \begin{array}{l} \mathrm{NH_{4}OAc(aq)} \\ 95^{\circ}\mathrm{C} \end{array}$$

$$\mathrm{(NH4)^{+}_{(x-1)}[Al_{(x-1)}Si_{(y+1)}O_{(2x+2y)}]^{(x-1)-} + (NH_{4})_{3}[AlF_{6}]}$$

Figure 9.2: XRD patterns of ZSM-5, BEA*, SSZ-35 and SSZ-25 before and after dealumination treatment. Bottom pattern is calcined material while top pattern is from the calcined dealuminated sample

A) ZSM-5 (Offset from difference in alignment of Instrument between measurements.)

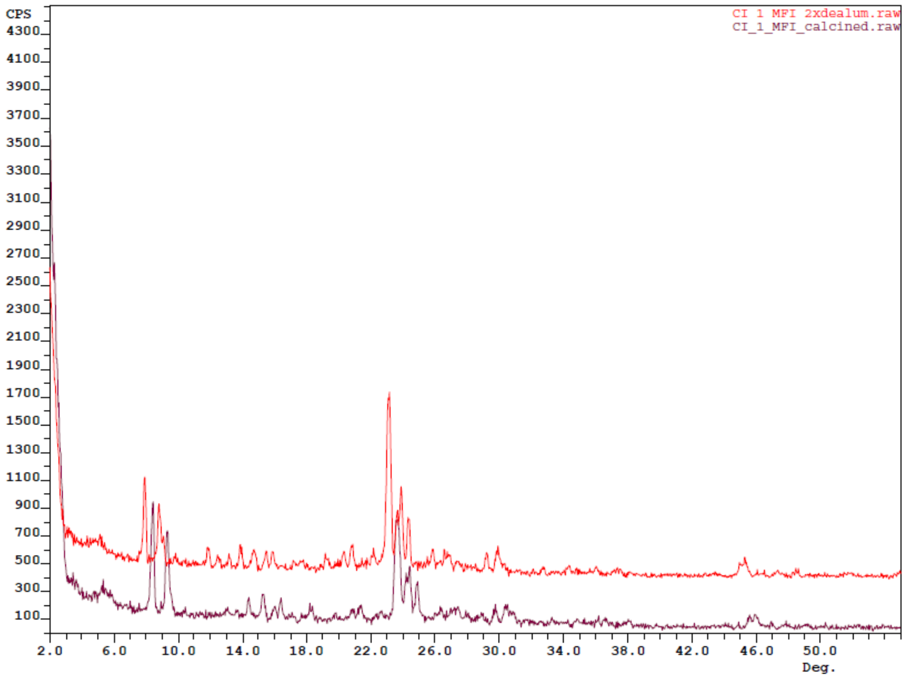

B) BEA*

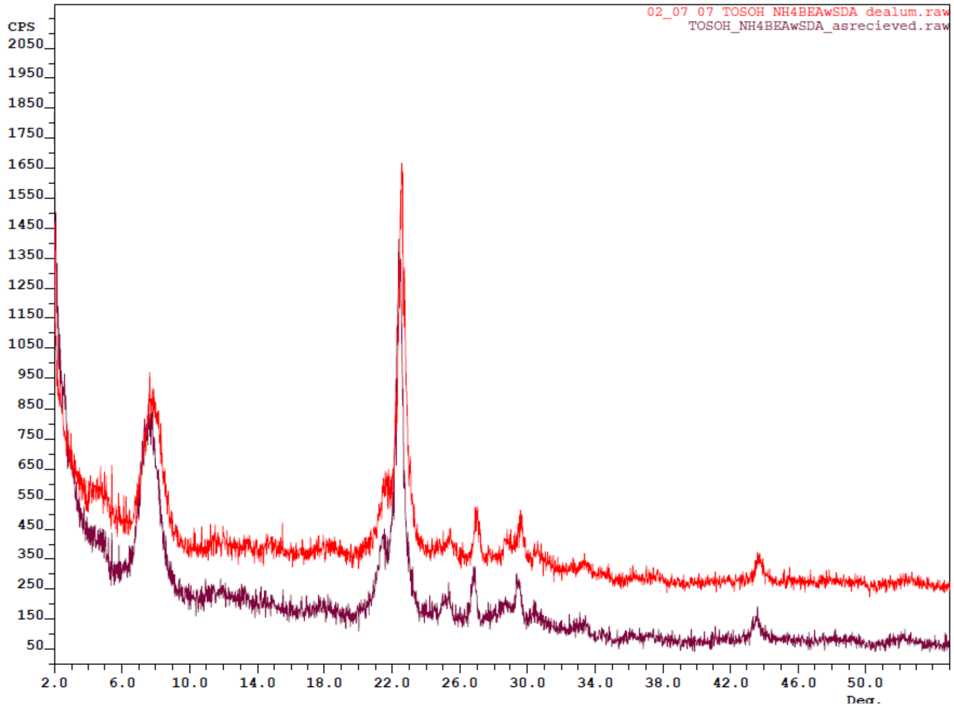

C) SSZ-35

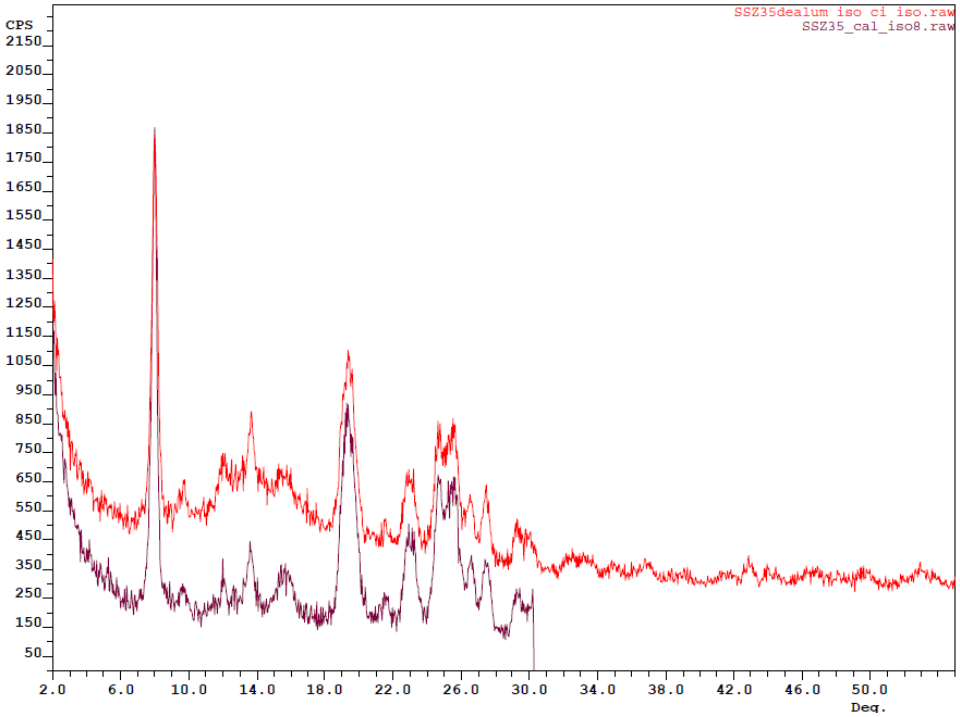

D) SSZ-25

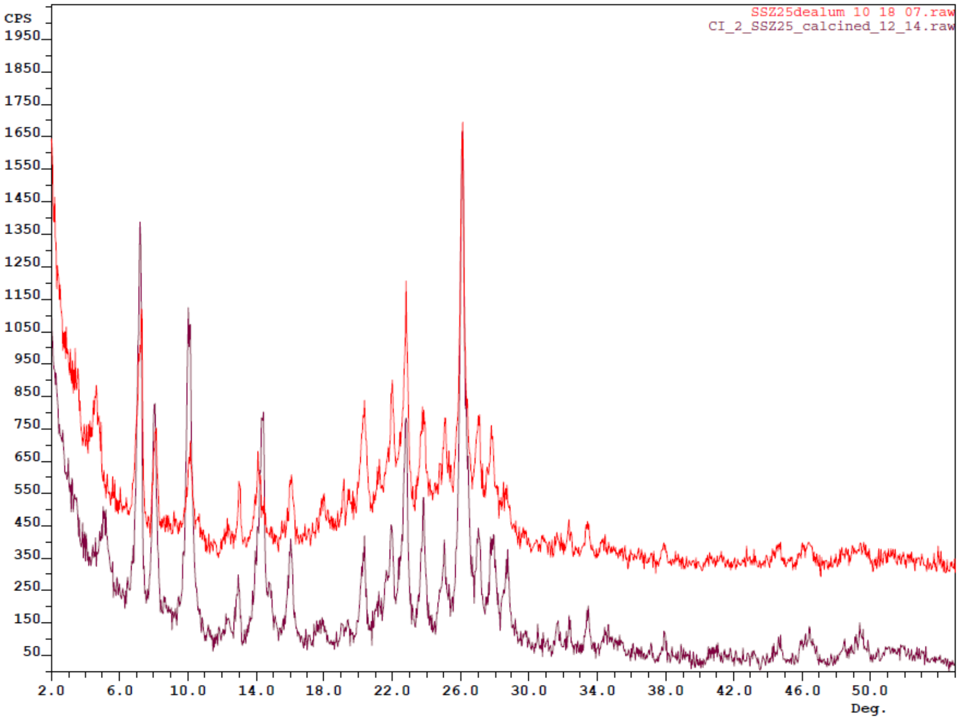

Figure 9.3: SEM images of ZSM-5, BEA*, SSZ-35, and SSZ-25 before and after dealumination procedure

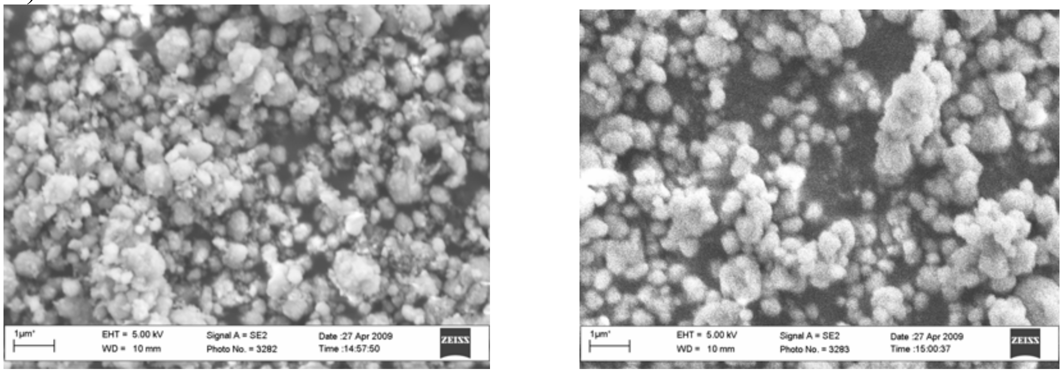

A) ZSM-5 As Made

ZSM-5 Dealuminated

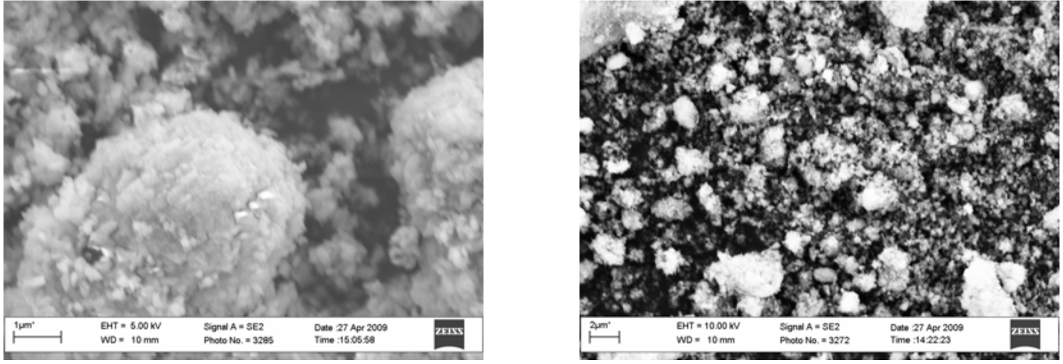

B) BEA* As Made

BEA* Dealuminated

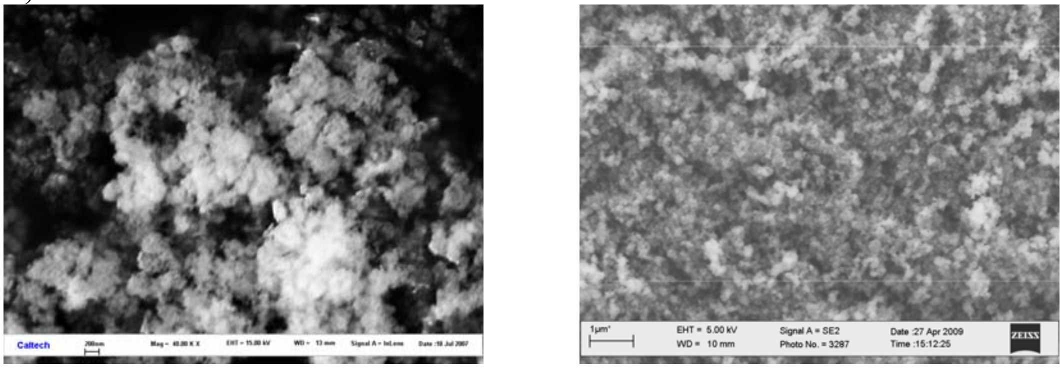

C) SSZ-35 As Made

SSZ-35 Dealuminated

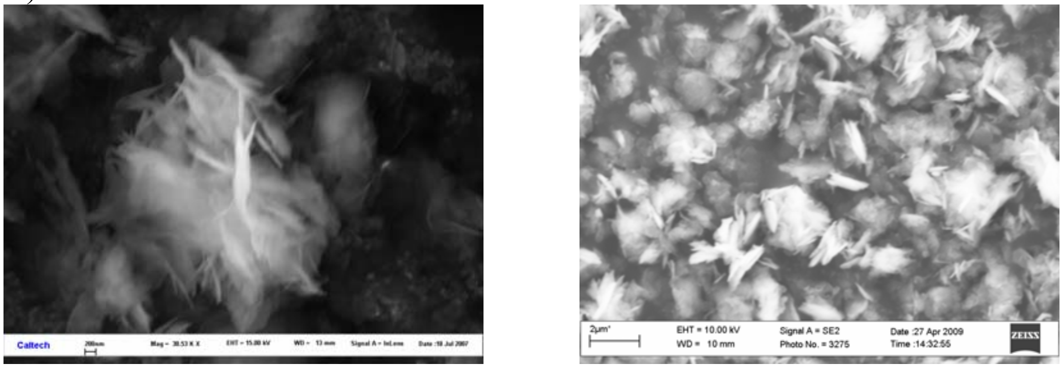

D) SSZ-25 As Made

SSZ-25 Dealuminated

Figure 9.4: TGA/DSC of ZSM-5, BEA*, and SSZ-35 demonstrating SDA degradation above 350°C

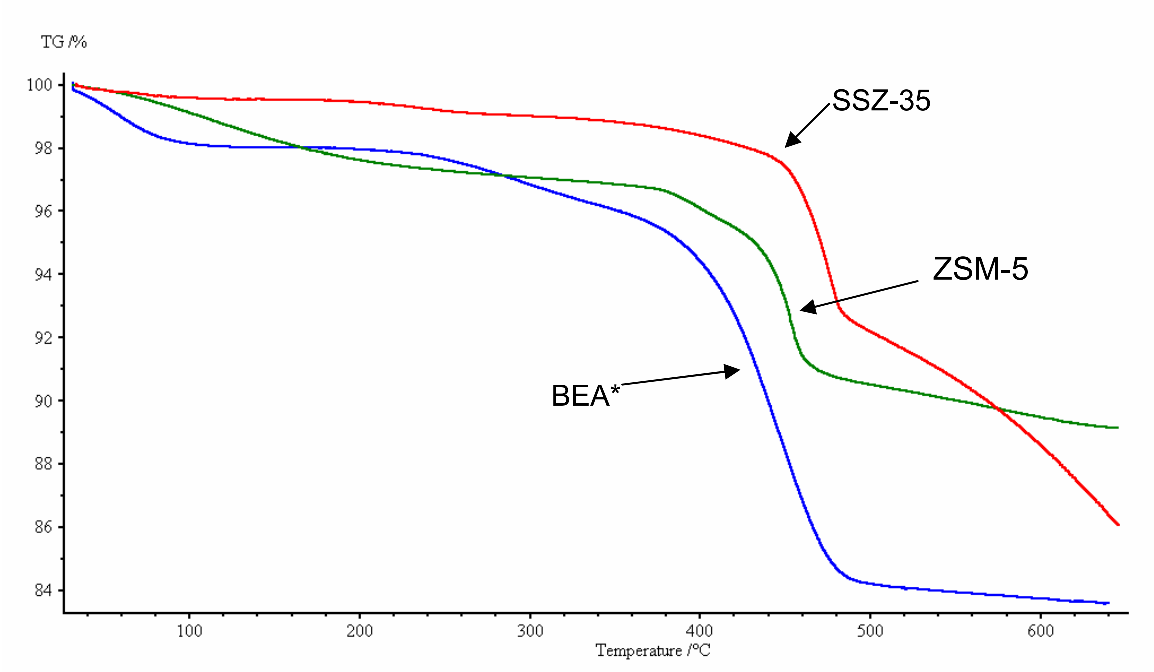

Figure 9.5: TGA/DSC of SSZ-25 demonstrating SDA degradation below 350°C.

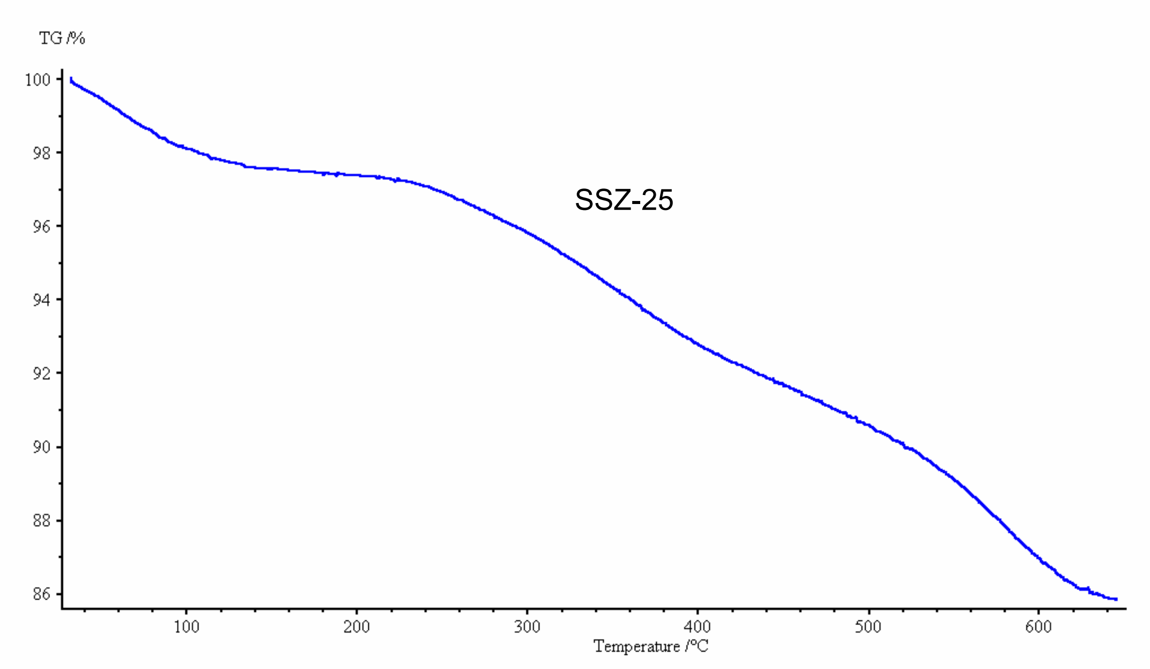

Figure 9.6: Isopropanol dehydration activity on the external surface of ZSM-5, BEA*, and SSZ-35 before and after dealumination treatment as well as calcined SSZ-35

Reactions were run using 0.5g zeolite, pelletized and crushed using a 20/40 mesh sieve. The Feed was 5 ml/min (room temp. measurement) of He/Ar and a liquid isopropanol feed rate of 10μl/min at atmospheric pressure and 150 °C."

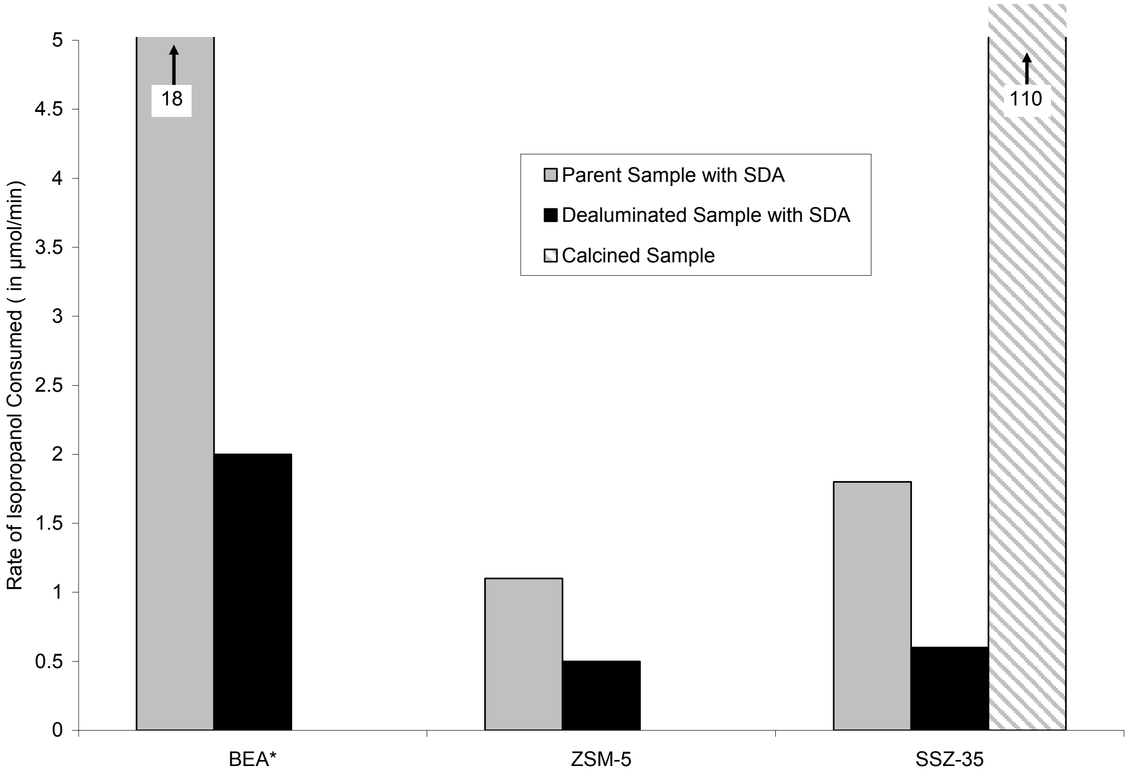

Figure 9.7: Constraint Index testing on zeolites before and after dealumination treatment

Reactions were run using 0.5g zeolite, pelletized and crushed using a 20/40 mesh sieve. The Feed was 5 ml/min (room temp. measurement) of He/Ar and a liquid 50 mol% n-hexane/50 mol% 3-methylpentane feed rate of 10μl/min at atmospheric pressure and 330 °C."

A)ZSM-5

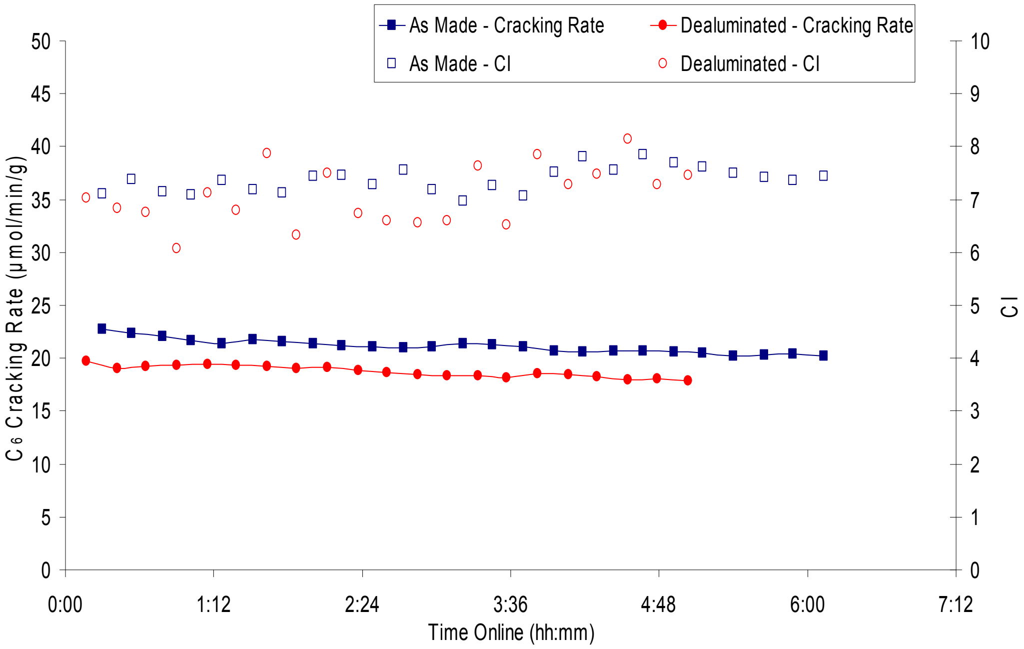

B) BEA*

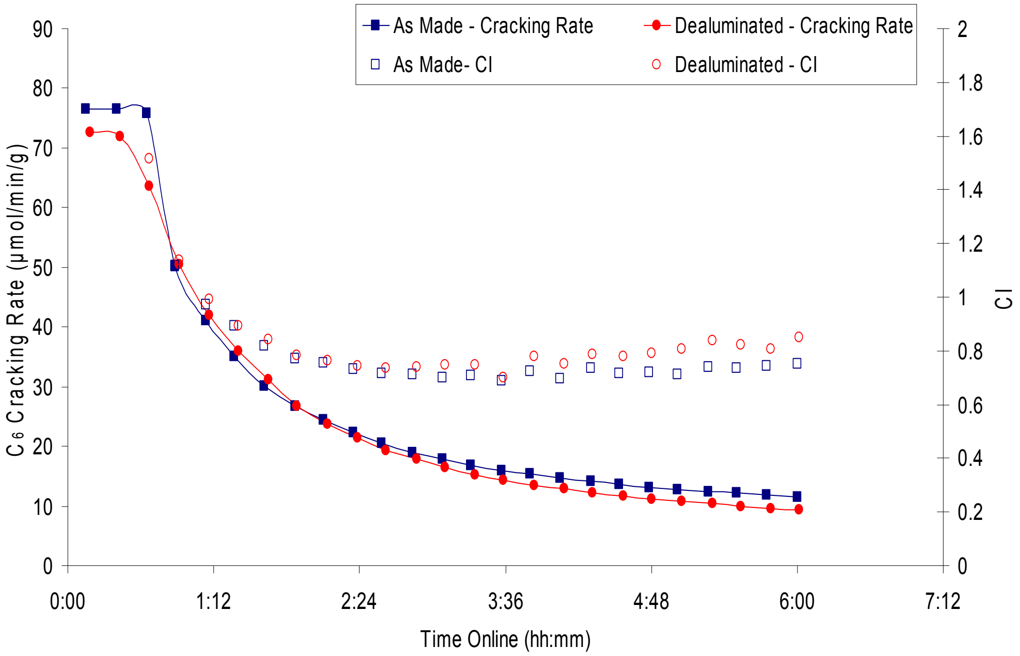

C) SSZ-35

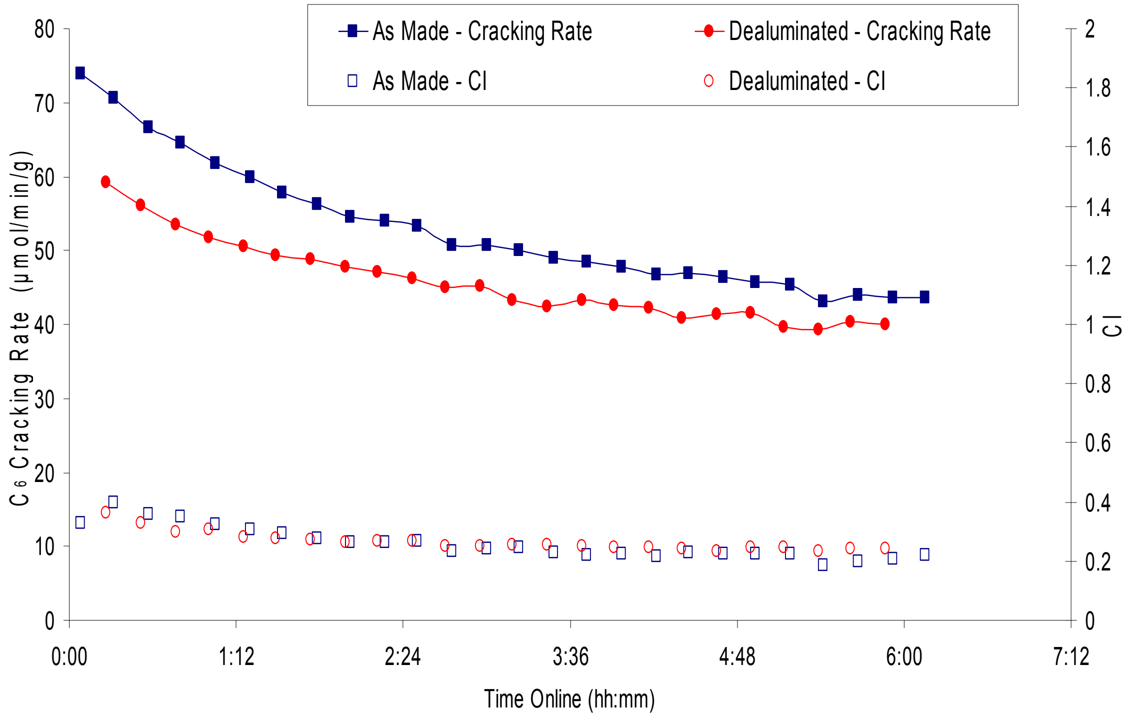

D) SSZ-25

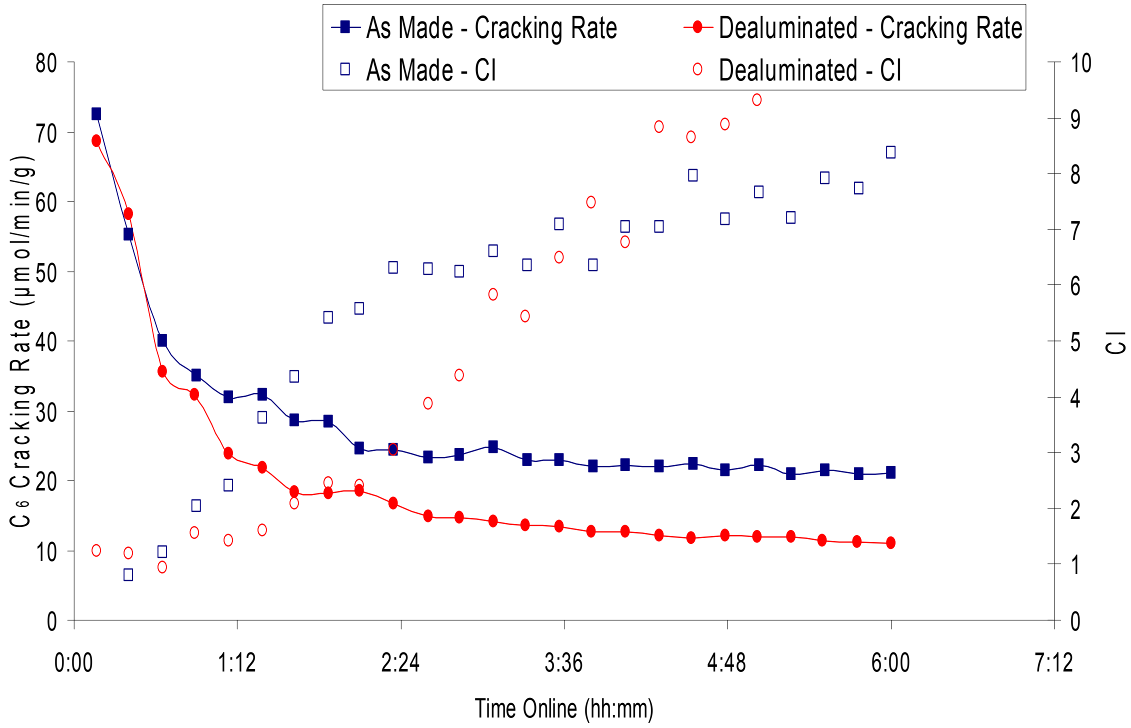

Table 9.1: Characterization data of zeolite samples before and after dealumination treatment (D-Denotes Dealuminated Samples)

.

Zeolite	**Surface Si/Al**[a]	**Bulk Si/Al**[b]	**Micropore Volume (cc/g)**[c]	**Crystal Size µm**
BEA	16.6	13.5	0.22	<0.25
D-BEA[d]	21.4	19.7	0.18	<0.25
ZSM-5	21.5	19.4	0.13	<0.5
D-ZSM-5[d]	30.1	19.8	0.11	<0.5
SSZ-25	18.2	16.0	0.13	0.5, thin plates
D-SSZ-25[d]	40.9	23.6	0.11	0.5, thin plates
SSZ-35	17.9	16.3	0.15	<0.1
D-SSZ-35[d]	26.4	20.2	0.11	<0.1

[a] Surface Si/Al determined by XPS. [b] Bulk Si/Al determined by ICP.
[c] Determined by t-plot method. [d] D- denotes dealuminated samples.

CHAPTER TEN

EVIDENCE OF INCREASED ACCESSIBILTY IN THE INTERIOR OF STRUCTURES WITH LARGE CAGES

With the external surface producing no discernable effect on the CI test for all of these structures, the effect of the cage on the accessibility of the internal structure to the reactant molecules and reaction transition-states must be considered. Zones and Harris raised this possibility in their observations of unusual results in the CI testing of zeolites[1]. Similarly the ability of reactant molecules to access the internal structure of a zeolite, as well as the limits on transition-states due to space around the active site, have been attributed to many observations of various forms of shape-selectivity[2]. Evidence of accessibility of n-hexane and 3-methylpentane can be viewed through adsorption experiments while transition state accessibility can lead to differences in deactivation and product selectivity.

10.1 Adsorption of n-Hexane and 3-Methylpentane

The uptake of hydrocarbons has been shown to be a useful tool in characterizing zeolites; such as the comparison of the rate of uptake of 2,2,-dimethylbutane on SSZ-57 and IM-5 with other known structures to gain insight into those structures.[3] In a similar manner the uptake of n-hexane and 3-methylpentane on the structures in this study may provide insight into their behavior and accessibility. Figure 10.1 depicts the adsorption of n-hexane and 3-methlypentane on the three 10-ring structures in this study; ZSM-5, SSZ-25, and SSZ-35. Across all three structures little discrimination is seen between the two adsorbates in the initial uptakes. Each of the initial uptakes is on a similar time scale and reaches >70% uptake in the first minute. ZSM-5 shows the largest difference in total uptake between adsorbates while both SSZ-25 and SSZ-35 have little difference in adsorption of the two molecules. For SSZ-35 it could be argued that this is due to the large pore of 5.7Å x 5.4Å [4], as opposed to 5.6Å x 5.3Å and 5.1Å x 4.1Å[4] for ZSM-5. However SSZ-25 (with pore sizes 5.5Å x 4.0Å and 5.1Å x 4.1Å[4]) shows the least discrimination between adsorbates even with the smallest pore size. For SSZ-25, it should be noted that the structure of SSZ-25 may have pore openings larger than the crystallographic portal size since the structure is believed to be formed by cross-linking layers during calcination which could result in incomplete cross-linking or misalignments that may not be seen by XRD and would increase the size of the pore openings. Looking at the adsorption on the smaller pore structures SSZ-23 and SSZ-28 in Figure 10.2, a larger resistance to uptake is observed. SSZ-23 with 9-ring pores with size 5.3Å x 3.7Å has a large distinction in the uptake between n-hexane and 3-methylpentane. However the CI value for SSZ-23 is lower than that of ZSM-5. This difference between adsorption selectivity and reaction selectivity highlights the cage effect on the CI test. It would be expected on the smaller pores of SSZ-23 that the 3-methylpentane reactant would be more hindered than on ZSM-5 and increase the observed CI value; however this is not the case. SSZ-28 also in Figure 10.2 shows decreasing adsorption with decreasing pore size, 8-rings of 4.4Å x 3.6Å[4], which would accountant for the lower activity than the 10-ring structures, but the CI value is still lower than that of ZSM-5. Adsorption profiles of these smaller pore structures do not correlate with the observed CI results for them.

10.2 Deactivation Characteristics of Caged Structures

As mentioned previously, another type of shape-selectivity observed in zeolites is transition-state selectivity [2]. This has been used to explain the results of the CI test on some structures [5], as well as the reason for ZSM-5's limited deactivation in hydrocarbon cracking[2]. Similarly the deactivation of n-heptane transformation has been shown to happen by coking limited to the large cages and not the sinusoidal channels [6]. It is not a hard stretch to visualize how the presence of cages in a structure would create large space around the active sites and fewer limitations on transition states. This increased transition state space is easily observed in looking at the deactivation of these structures over time in the CI test. Looking back at Figure 9.7, ZSM-5's activity remains fairly constant over 6h online while the other 10-ring structures and BEA* show larger deactivation. Similarly deactivation is seen in the small pore structures as well in Figure 10.3. Table 10.1 shows a closer look at the deactivation on the basis of mass accumulation in the structure over time on stream at 1h and 6h time points. ZSM-5, while experiencing an accumulation of mass, does so to a lesser degree than either of the other 10-ring structures when looked at on a per-site basis and less deposition per amount of reactant cracked (Figure 10.4). All of the caged structures continue to have mass accumulation at a larger rate than ZSM-5. Extrapolating the data from Table 10.1 to 8.2 mmol C6 cracked/mmol Al for all samples, the g deposited/mmol Al ranks the structures as ZSM5<SSZ-25<SSZ-28<SSZ-35<SSZ-23 at 39.6, 42.1,42.6,46.6, and 53.8 g/mmol Al, respectively. They show a larger tendency than ZSM-5 toward carbon deposition which can be attributed to the larger transition-state space afforded by the larger cages in the structures. The accumulation can be attributed to the internal void spaces by looking at the reduction in micropore volume for each sample. SSZ-25 and SSZ-35 both show micropore volume reductions greater than 80% of the volume of the parent material while ZSM-5 remains relatively open with only a 15% reduction in micropore volume.

XPS and elemental analysis of the deactivated samples show consistent trends as those observed by thermal gravimetric analysis. Table 10.1 also shows the ratio of C/(Si +Al) for the samples. ZSM-5 shows the smallest increase in carbon from 1h to 6h with an increase of 50% while SSZ-35 has a 60% increase and the other samples increase at least 80%. By XPS analysis, the surface increases are smaller for all samples and actually decrease for SSZ-35 and SSZ-28. The XPS analysis and elemental analysis showed the most similar change on ZSM-5 than for the other samples.

Looking at the increase in carbon content from both XPS and elemental analysis provides insight into the location of the deposition. XPS analysis only looks at the carbon deposition near the surface of the zeolite and can be attributed mainly to accumulation on the external surface. Elemental analysis on the other hand provides information on the entire sample. Identical increases would be observed for deposition only on the external surface while interior build up would result in a higher value from elemental analysis. For ZSM-5 this the mol% carbon of the sample shows a 50% increase by elemental analysis and a 30% increase for XPS analysis, suggesting interior deposition is suppressed as expected. For SSZ-35, a 60% carbon increase is observed for the bulk and the surface actually has a 30% decrease, for SSZ-25 the increases are 80% for the bulk and 30% for the surface, for SSZ-23 the increases are 90% for the bulk and 2% for the surface and for SSZ-28 the bulk has a 90% increase in the carbon while like SSZ-35 a 30% decrease is observed by XPS. As can be seen the XPS data includes two decreases in the surface carbon content. A closer inspection of the data reveals that for all samples the data was spread out over a large range, the problems in reproducibly have partially been attributed some to difficulty in focusing the x-ray spot onto only the coked crystals. In fact the data from data for each sample from the 1h time point overlap with the 6h time point suggesting that the surface content between the two is similar and the increases in the carbon content are closer to 0% and thus still evidence that the carbon accumulation in the samples is internal to the structure. All of these values suggest larger internal deposition than seen in ZSM-5 indicating there is significant accumulation of carbon species internally in the structures and that the micropore volume reductions are from lost internal space rather than just external pore blockage. The ratios for SSZ-25 would most likely show a larger difference if an earlier time point had been used because, as can be seen in Figure 9.7d, a large portion of the deactivation attributed to the large cage has already occurred by the 1 hour time point. These increases would also indicate the larger space of the cages provide fewer limitations to the formation of the deactivating carbon species than in ZSM-5. This would be indicative of less transition-state selectivity in the CI test for these zeolites than in ZSM-5, which would result in lower CI values for these zeolites than ZSM-5 even with smaller or similar pore openings.

10.3 Hydrocarbon Cracking in Caged Structures

Another aspect in which we can see the cage effect comes from looking at the cracking of n-hexane and 3-methylpentane individually on the structures of SSZ-23, SSZ-25, and SSZ-28 in Figure 10.3. For the small pore structures of SSZ-23 and SSZ-28 the reaction rate is much lower than the larger 10-ring structures shown, however the similarity in reactivity between n-hexane and 3-methylpentane suggest that 3-methylpentane is reacting on internal sites as opposed to external sites. Also while isomerization of the 3-

methylpentane to n-hexane is possible, the i-C_4/*n*-C_4 ratios indicate a different product distribution for 3-methylpentane cracking than n-hexane cracking on SSZ-23 or SSZ-28. If the 3-methylpentane were reacting by undergoing isomerization to n-hexane then cracking similar product distributions to n-hexane cracking would be expected. On SSZ-23, the i-C_4/*n*-C_4 ratio is 0.7 for n-hexane cracking and around 2.0 for 3-methylpentane cracking. SSZ-28 had ratios of 0.5 and 1.7, respectively. In the CI test this ratio was 1.4 for SSZ-23 and 1.1 for SSZ-28 which are more similar to the 10-ring structures like ZSM-5 than the reported value of 0.14 for the 8-ring structure SSZ-13[1]. It was also observed in this study that the external surface of a completely pore blocked structure of SSZ-35 showed no reactivity on the external surface after only 15 minutes online. SSZ-23's higher initial n-hexane activity can be attributed to the large disparity in uptake seen between n-hexane and 3-methlypentane in the adsorption results in Figure 10.2. As with SSZ-23, SSZ-28 shows a larger deactivation with n-hexane cracking than 3-methylpentane cracking. There may be a limit on the formation of deactivation species from 3-methylpentane, much like the limit seen in ZSM-5 but for the smaller n-hexane the limit is reduced leading to more deactivation for n-hexane cracking. SSZ-25 provides a unique opportunity to look at the contribution of the cage due to the presence of two separate pore systems in the structure, a series of cages connected by 10-rings and a separate set of 10-ring sinusoidal channels. As seen in Figure 10.2, initially SSZ-25 shows a very high activity with little difference in the activity for 3-methylpentane or n-hexane cracking. However, as the system deactivates, a higher level of activity remains for n-hexane than 3-methylpentane. Since the pore size of SSZ-25 is smaller than that of ZSM5, it is reasonable to consider the sinusoidal channel system would have limited deactivation and favor n-hexane cracking like ZSM-5, and the large cages is where the majority of deactivation and carbon species accumulation occurs. As is seen in Figure 10.2, this is what happens as the cage system deactivates the reaction profile shifts from looking like a large pore structure to a medium pore structure like ZSM-5. The effect of internal cages in lowering selectivity in the CI test by increasing accessibility to reactants and transition-states is evident through these results.

10.4 References

[1] S.I. Zones, T.V. Harris, Micro. Meso. Mater. 31 (2000) 35.

[2] A.M. Rigby, G.J. Kramer, R.A. Van Santen, J. Catal. 170 (1997) 1.

[3] S.I. Zones, C.Y. Chen, A. Corma, M.T. Cheng, C.L. Kibby, I.Y. Chan, A.W. Burton, J. Catal. 250 (2007) 41.

[4] M.V. Frash, R.A. Van Santen, Topics Catal. 9 (1999) 191.

[5] A. Corma, A.V. Orchilles, Micro. Meso. Mat. 35 – 36 (2000) 21.

[6] P. Matias, J.M. Lopes, S. Laforge, P. Magnoux, M. Guisnet, F.R. Ribeiro, Appl. Catal. A: Gen. 351 (2008) 174.

Figure 10.1: Adsorption of n-hexane and 3-methylpentane on 10-ring pore structures

Adsorption measurements made at P/P_o of 0.3 on a Cahn C-2000 balance in the manner detailed by Chen in previous work[7].

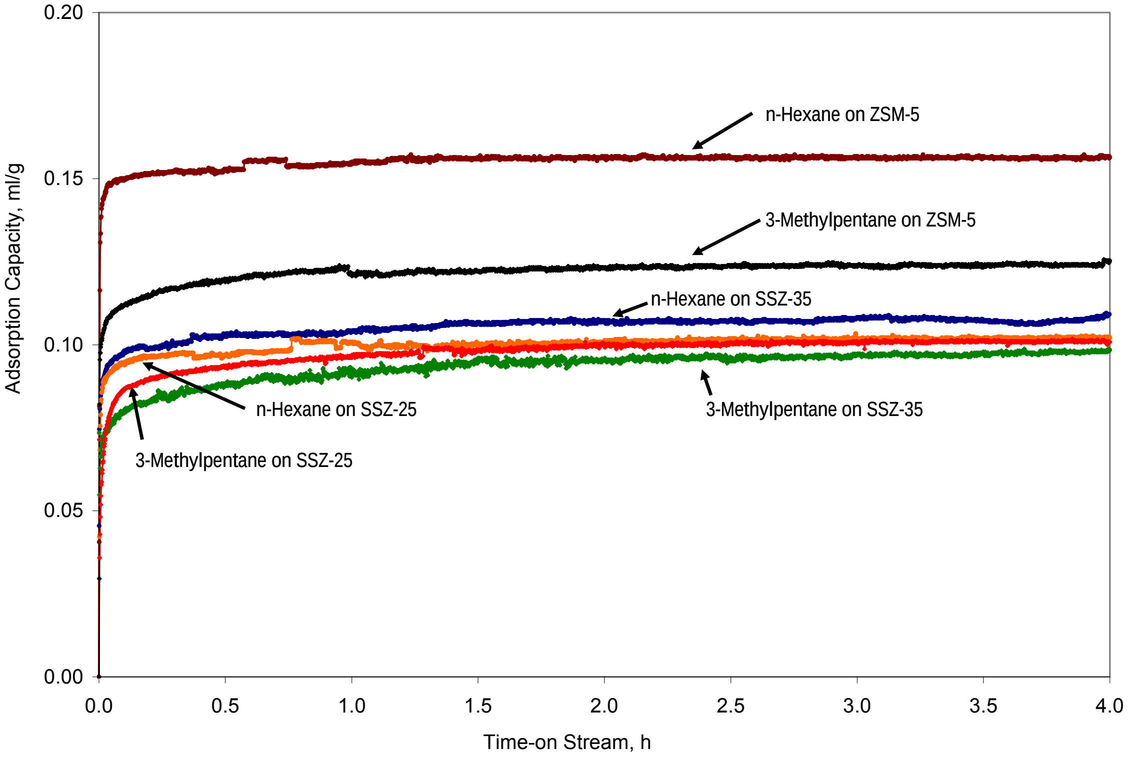

Figure 10.2: Adsorption of n-hexane and 3-methylpentane on small pore structures Adsorption measurements made at P/P$_o$ of 0.3 on a Cahn C-2000 balance in the manner detailed by Chen in previous work[7].

A) SSZ-23

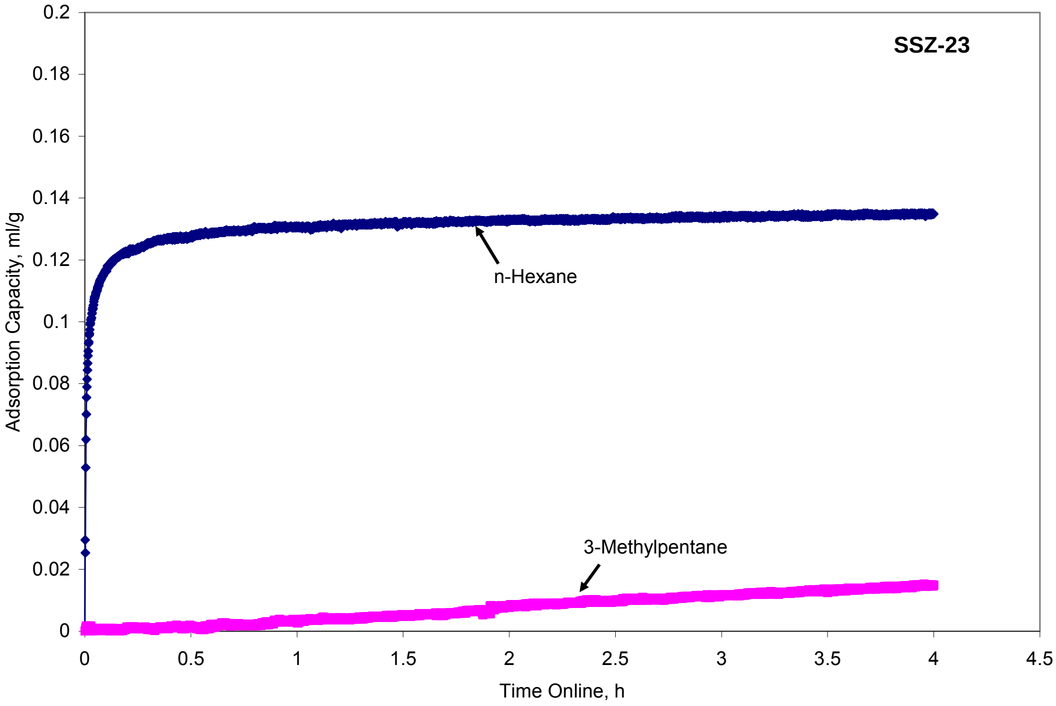

B) SSZ-28

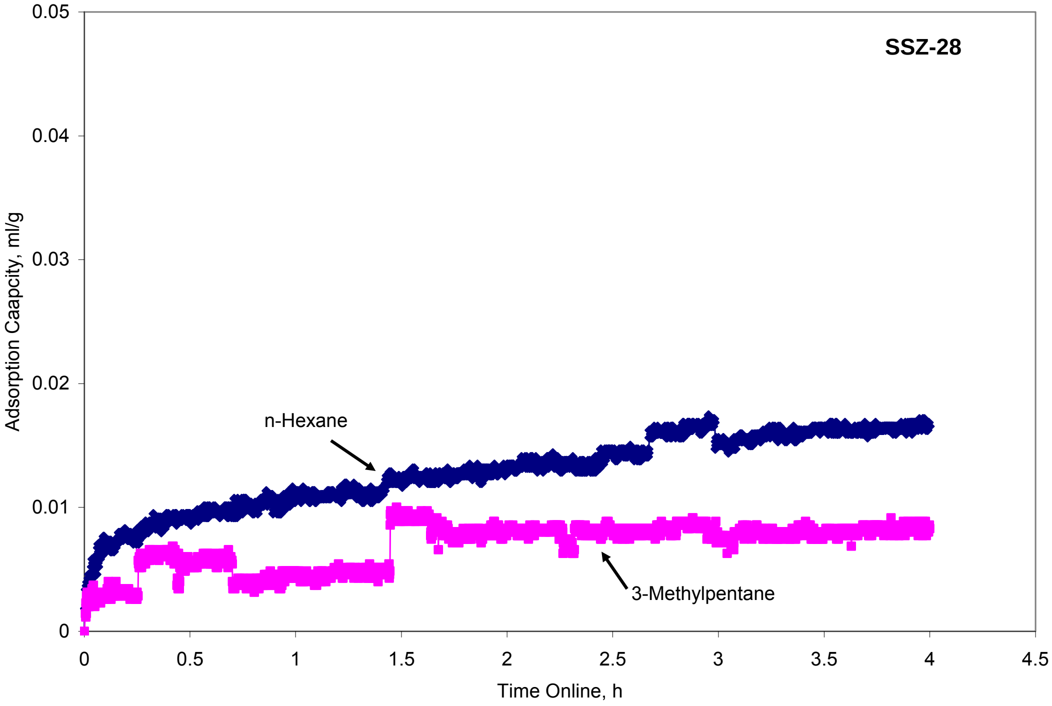

Figure 10.3: Constraint Index and cracking rate of individual pure reactants over time on stream for the small pore structures SSZ-23 and SSZ-28 as well as SSZ-25

Reactions were run using 0.5g zeolite, pelletized and crushed using a 20/40 mesh sieve. The Feed was 5 ml/min (room temp. measurement) of He/Ar and a liquid 50 mol% n-hexane/50 mol% 3-methylpentane feed rate of 10µl/min at atmospheric pressure. SSZ-25 was run at 330 °C while SSZ-23 and SSZ-28 were run at 375 °C."

A) SSZ-23 (375°C)

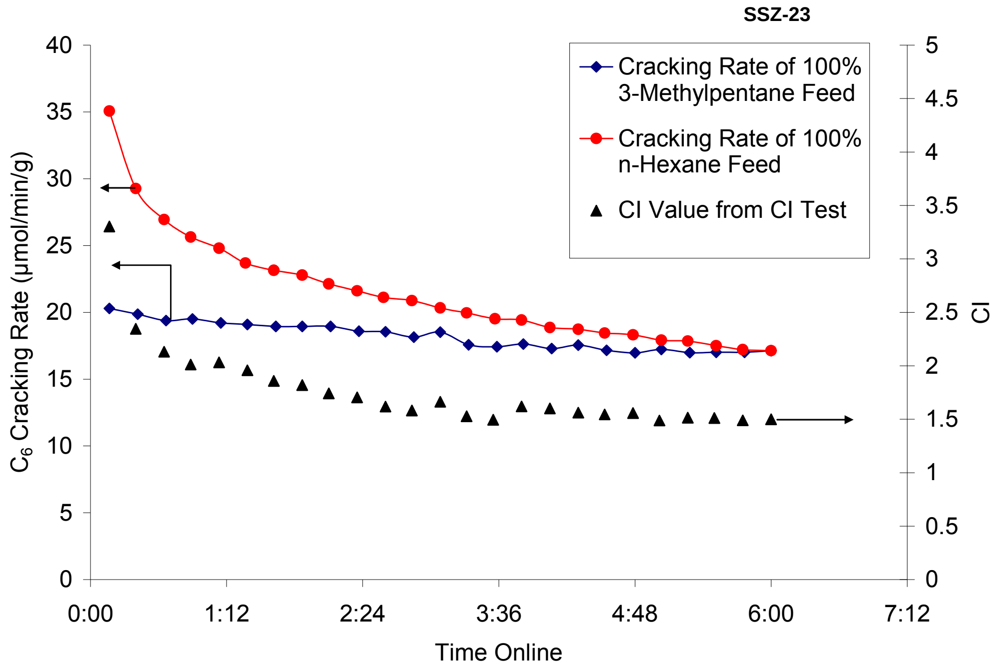

B) SSZ-28 (375°C)

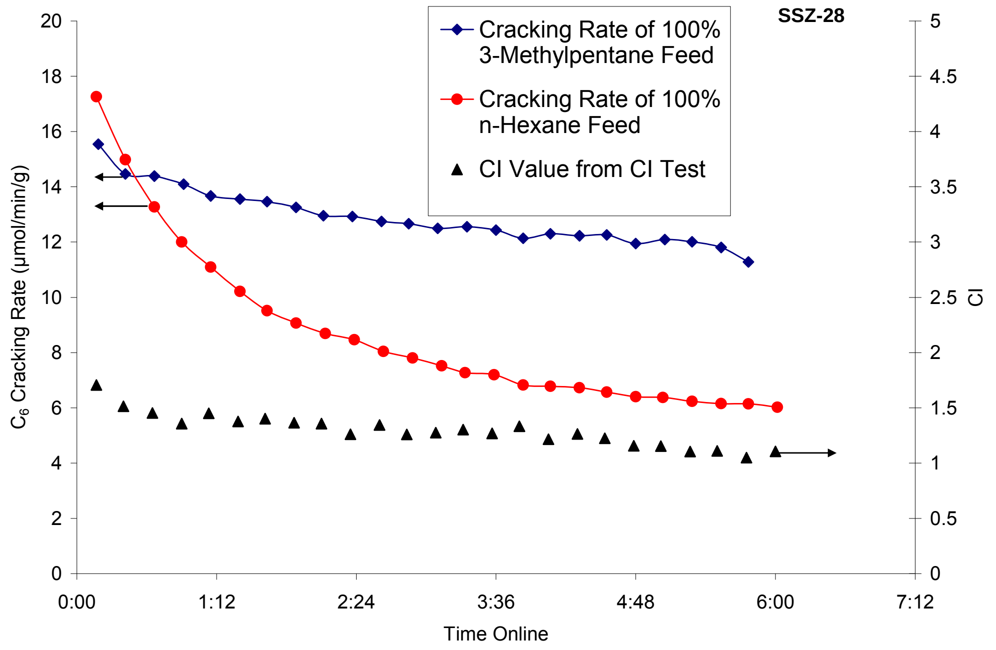

C) SSZ-25 (330°C)

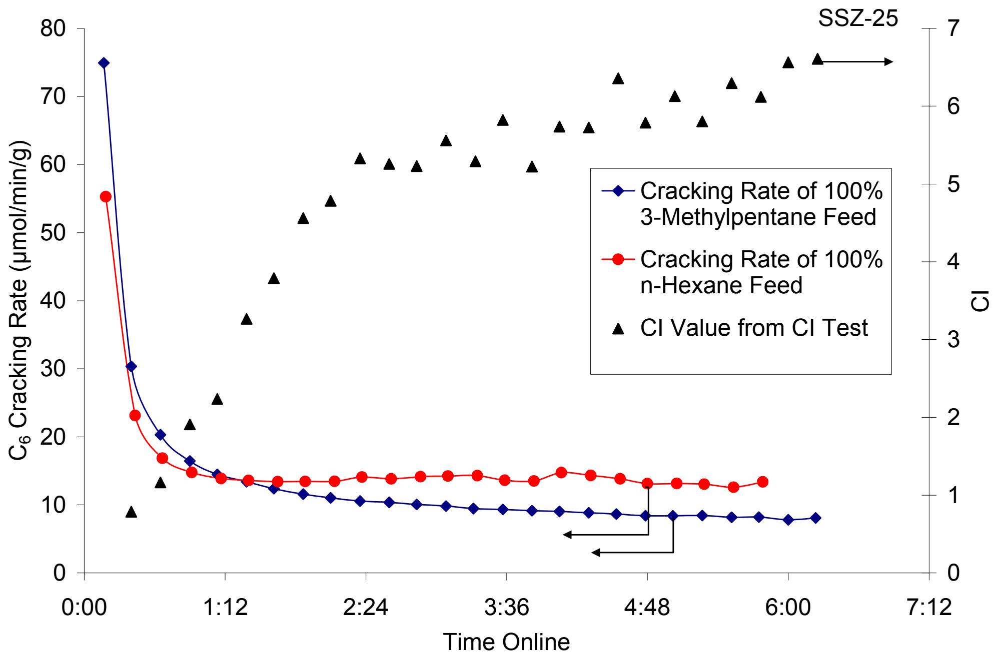
SSZ-25
C6 Cracking Rate (µmol/min/g)
0
10
20
30
40
50
60
70
80
CI
0
1
2
3
4
5
6
7
Time Online
0:00
1:12
2:24
3:36
4:48
6:00
7:12
Cracking Rate of 100% 3-Methylpentane Feed
Cracking Rate of 100% n-Hexane Feed
CI Value from CI Test

Figure 10.4 Comparison of mass accumulation on structures with the amount of C_6 cracked on those structures during Constraint Index testing

Reactions were run using 0.5g zeolite, pelletized and crushed using a 20/40 mesh sieve. The Feed was 5 ml/min (room temp. measurement) of He/Ar and a liquid 50 mol% n-hexane/50 mol% 3-methylpentane feed rate of 10μl/min at atmospheric pressure. ZSM-5, SSZ-35 and SSZ-25 were run at 330 °C while SSZ-23 and SSZ-28 were run at 375 °C."

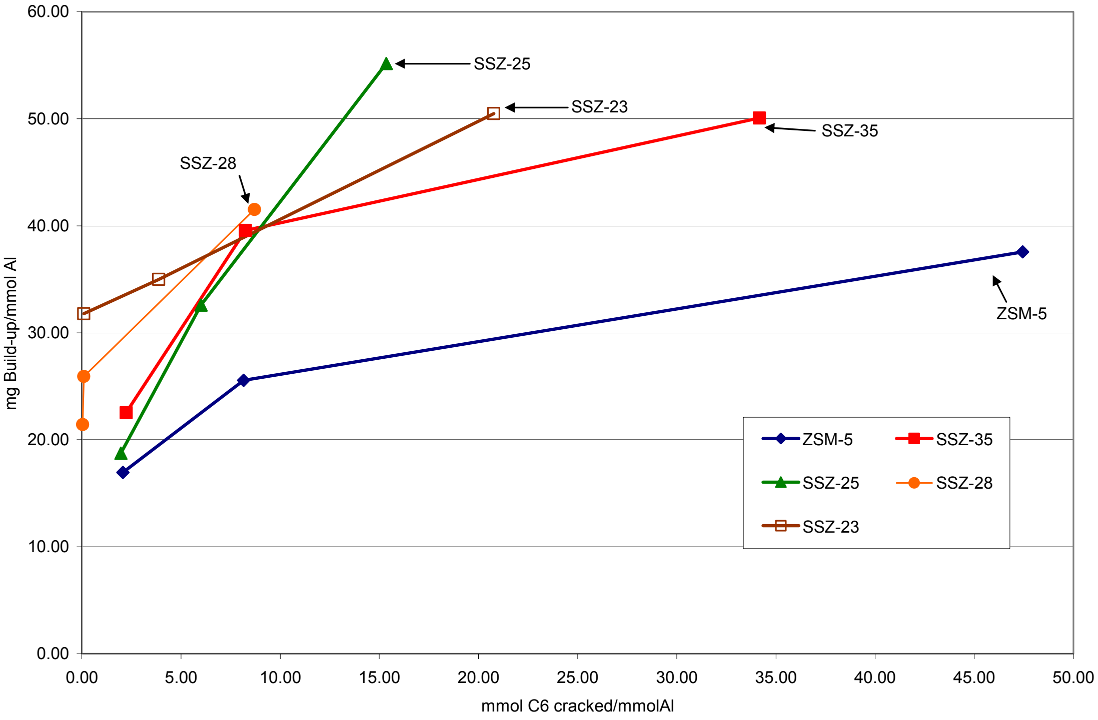

Table 10.1: Characterization of mass deposition from samples at the 1h and 6h time point in the Constraint Index test

Zeolite	Time on Stream	mmols C_6 Cracked[f]		Mass Deposited mg of mass		Micropore Vol. ml/g zeolite[b]	% Carbon Increase from 1h to 6h on Stream	
		/g zeolite	/mmol Al[a]	/g zeolite	/mmol Al[a]	(% reduced)[c]	Bulk[d]	Surface[e,g]
ZSM-5	1h	5.5	8.2	26.7	39.6			
	6h	32	47	31.3	46.4	0.11 (15%)	50%	30%
SSZ-35	1h	7.0	8.3	39.6	46.7			
	6h	29	34	56.9	67.0	0.03 (80%)	60%	-30%
SSZ-25	1h	5.1	6.0	33.8	37.1			
	6h	14	15	52.7	57.8	0.02 (85%)	80%	30%
SSZ-23	1h	1.4	3.9	16.6	46.0			
	6h	7.5	21	27.8	77.0	0.11 (31%)	90%	20%
SSZ-28	1h	0.045	0.10	15.8	34.4			
	6h	4.0	8.7	19.8	43.1	0.10 (33%)	90%	-30%

[a] mmols Al determined from elemental analysis, assumes all Al is in the framework

[b] Determined by N_2 adsorption

[c] % reduced as compared with calcined parent sample

[d] Determined from elemental analysis

[e] Determined from XPS measuring the near surface region

[f] ZSM-5, SSZ-35 and SSZ-25 were tested at a reaction temperature of 330°C while SSZ-23 and SSZ-28 were at 375°C.

[g] The XPS data for 1h and 6h carbon content fell within a standard deviation of each other and the data range was fairly wide. The points are likely much closer to 0%

CHAPTER ELEVEN

EVIDENCE OF MULITPLE STRUCTURE FEATURES IN CONSTRAINT INDEX TESTING

Besides the lower than expected Constraint Index values seen on the structures with large cages, another unique feature of the Constraint Index test observed was the change in the value for the SSZ-25 structure. Zones and Harris [1] interpret this behavior as the expression of the difference in fouling rates for the two pore systems in the structure. This again is consistent with the work of Guisnet on n-heptane transformation over MCM-22 (the same **MWW** structure as SSZ-25).[2] A similar behavior in the Constraint Index test over time on stream has been observed for offretite.[3] Again this result is interpreted to be due to the fouling of the larger 12-ring channels while slower deactivation in the gmelinite cages is observed. This is observed by poisoning the feed with pyridine and observing an increased initial CI value for the same sample.[3]

Typically the Constraint Index value is reported at one time point between 20 and 40 minutes online. However based on these two observations, the Constraint Index test may also provide evidence indicating the presence of different features in structures, i.e., different pore systems, different pore sizes, additional cages, etc. Figure 11.1 shows the Constraint Index behavior over time on stream for various structures. The structures of MOR and FER each have multiple features show similar changing Constraint Index over time; while MOR increases much like offretite and SSZ-25, FER shows a large decrease. Fouling of the catalyst alone does not result in the changing behavior of the Constraint Index. USY and BEA* both have large-pore 3-dimensional structures that quickly foul but maintain a similar Constraint Index value over 6 hours online. Similarly the 1-dimensional structure of ZSM-12 has large pores that show quick fouling but also maintains a fairly constant Constraint Index value over 6 hours online. The Constraint

Index of ZSM-12 is slightly higher than expected for 12-ring structures; this is attributed to the smaller pore sizes of ZSM-12 compared to other 12-ring structures and having no internal intersections. The behavior of MOR (Si/Al ~6.5) can be explained similar to that of SSZ-25 and offretite where the large 12-ring channel fouls and the influence of the smaller side cages contributes to an increasing Constraint Index value. FER on the other hand shows a decrease which may be attributed to the distribution of sites in the smaller 8-ring cages and the 10-ring channels which can vary based on synthesis method.[4,5,6] Figure 11.2 shows the fractions of n-hexane and 3-methylpentane remaining in the Constraint Index test over MOR(Si/Al ~6.5), FER, and SSZ-25. In the case of the MOR and SSZ-25 there is initial fouling and decrease in the activity of both n-hexane and 3-methylpentane. Then the cracking rate of n-hexane levels off to a quasi-steady level while the cracking rate of 3-methylpentane drops further. In FER however the cracking rate of 3-methylpentane is constant over the run, while a decrease in n-hexane occurs resulting in the dropping Constraint Index value.

Several studies have shown through adsorption experiments n-hexane does not enter the small cages of ferrierite [7,8] or the side pocket of MOR[5]. This would suggest that the CI time dependence for these materials does not arise from the different features in the structure as the small cages and side pockets might not be accessed by the reactants. However these adsorption experiments occur at temperatures lower than the reaction conditions of the CI test. Distinguishing the ability of n-hexane and 3-methylpentane to enter the small cages and side pockets under reaction conditions would provide better insight. This can be accomplished by limiting the reaction to one feature of each structure.

Various work has shown that Na^+ cations preferentially exchange into the 8-ring side pockets in MOR.[5,9,10] Similarly, Na^+ cations preferentially exchange into the small channels of ferrierite.[11] Using the same ion-exchange conditions as the Igelsia work partial Na+ exchanges were performed on the MOR(Si/Al ~6.5) and FER and then tested in the Constraint Index test. Figure 11.3 demonstrates the results of those tests. In the MOR sample the Constraint Index value remains low at a level not unexpected for a large pore zeolite over the entire length of the run and the cracking rate is less than half the cracking rate of the as-made sample. In the FER sample, partial Na^+ exchange depressed the initial Constraint Index values to a level expected for that of a 10-ring zeolite and that level is maintained over the entire run. The conflicting results of these Constraint Index results with the adsorption studies demonstrating n-hexane can not enter the small cages and side pockets of ferrierite and mordenite, respectively, may be explained by the difference in experimental temperature of the Constraint Index test and the adsorption experiments. Looking further at the ferrierite sample reducing the temperature to 375°C reduces the Constraint Index value as shown in Figure 11.4. In these two tests the cracking rate of 3-methylpentane is similar but the cracking rate of n-hexane decreases with decreasing temperature. If a shift from monomolecular to bimolecular cracking were occurring, the Constraint Index would be expected to increase, much like that observed by Haag on ZSM-5 over temperature.[12] Ferrierite shows the opposite, suggesting a reduction in the ability of n-hexane to reach some sites.

While these are examples of evidence of multiple features by Constraint Index testing that may not always be the case. A sample of MOR also from Zeolyst but with a Si/Al ~ 10 showed no increase in the Constraint Index behavior over 6 hours on stream at the same conditions. Room exists for future exploration into the differences between these mordenite samples. Similarly methods to eliminate the sites in the large channels would provide more evidence of the influence of sites in the smaller channels and cages of ferrierite and mordenite. The Constraint Index test has the ability to provide insight into multiple features of a structure by observing changes in the Constraint Index over time, but the absence of change does not rule out multiple features.

11.1 References

[1] S.I. Zones, T.V. Harris, Micro. Meso. Mater. 31 (2000) 35.

[2] P. Matias, J.M. Lopes, S. Laforge, P. Magnoux, M. Guisnet, F.R. Ribeiro, Appl. Catal. A: Gen. 351 (2008) 174.

[3] F.R. Ribeiro, F. Lemos, G. Perot, M. Guisnet, in R.Setton (ed.) Chemical Reactions in Organic and Inorganic Systems, Reidel Pub. Co., (1986) 141.

[4] V.L. Zholobenko, D.B. Lukyanov, J. Dwyer, W.J. Smith, J. Phy. Chem. B. 102 (1998) 2715.

[5] A. Bhan, A.D. Allian, G.J. Sunley, D.J. Law, E. Iglesia, J. Am. Chem. Soc. 129 (2007) 4919.

[6] A.B. Pinar, C. Marquez-Alvarez, M. Grande-Casas, J. Perez-Pariente, J. Catal 263 (2009) 258.

[7] W.J.M. van Well, X. Cottin, J.W. de Haan, B. Smit, G. Nivarthy, J.A. Lercher, J.H.C. van Hooff, R.A. van Santen, J. Phys. Chem. B 102 (1998) 3945.

[8] W.J.M. van Well, X. Cottin, B. Smit, J.H.C. van Hooff, R.A. van Santen, J. Phys. Chem. B 102 (1998) 3952.

[9] M.A. Makarova, A.E. Wilson, B.J. van Liemt, C. Mesters, A.W. de Winter, C.J. Williams, J. Catal. 172 (1997) 170.

[10] V.A. Veefkind, M.L. Smidt, J.A. Lercher, Appl. Catal., A 194 (2000) 319.

[11] B. Wichterlova, N. Zilkova, E. Uvarova, J. Cejka, P. Sarv, C. Paganini, J.A. Lercher, App. Cat., A 182 (1999) 297.

[12] V.J. Frillette, W.O. Haag, R.M. Lago, J. Catal. 67 (1981) 218.

Figure 11.1 Constraint Index test over time on stream for various zeolite structures
Reactions were run using 0.5g zeolite, pelletized and crushed using a 20/40 mesh sieve. The Feed was 5 ml/min (room temp. measurement) of He/Ar and a liquid 50 mol% n-hexane/50 mol% 3-methylpentane feed rate of 10μl/min at atmospheric pressure. ZSM-5, SSZ-35, BEA*, SSZ-25 and USY were run at 330 °C. MOR, FER, SSZ-23, SSZ-28 and ZSM-12 were run at 375 °C.

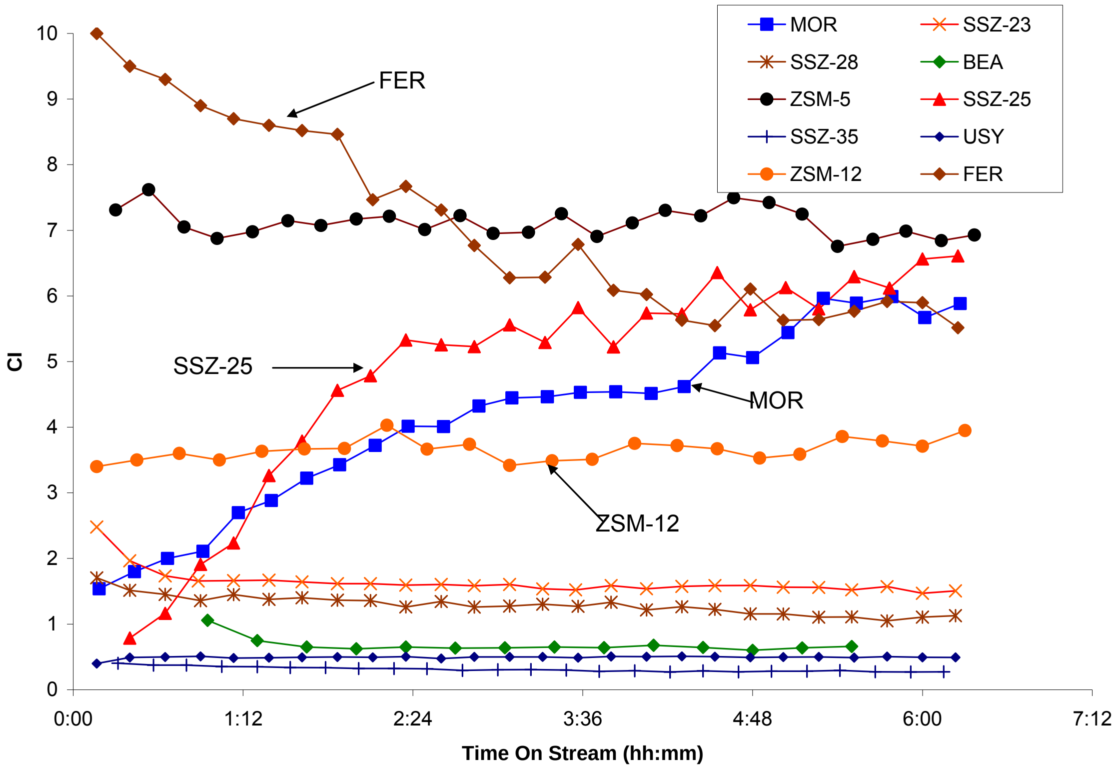

Figure 11.2: Fraction of n-hexane and 3-methylpentane remaining during the Constraint Index test on MOR, FER, and SSZ-25

Reactions were run using 0.5g zeolite, pelletized and crushed using a 20/40 mesh sieve. The Feed was 5 ml/min (room temp. measurement) of He/Ar and a liquid 50 mol% n-hexane/50 mol% 3-methylpentane feed rate of 10μl/min at atmospheric pressure. SSZ-25 was run at 330 °C while SSZ-23 and SSZ-28 were run at 375 °C."

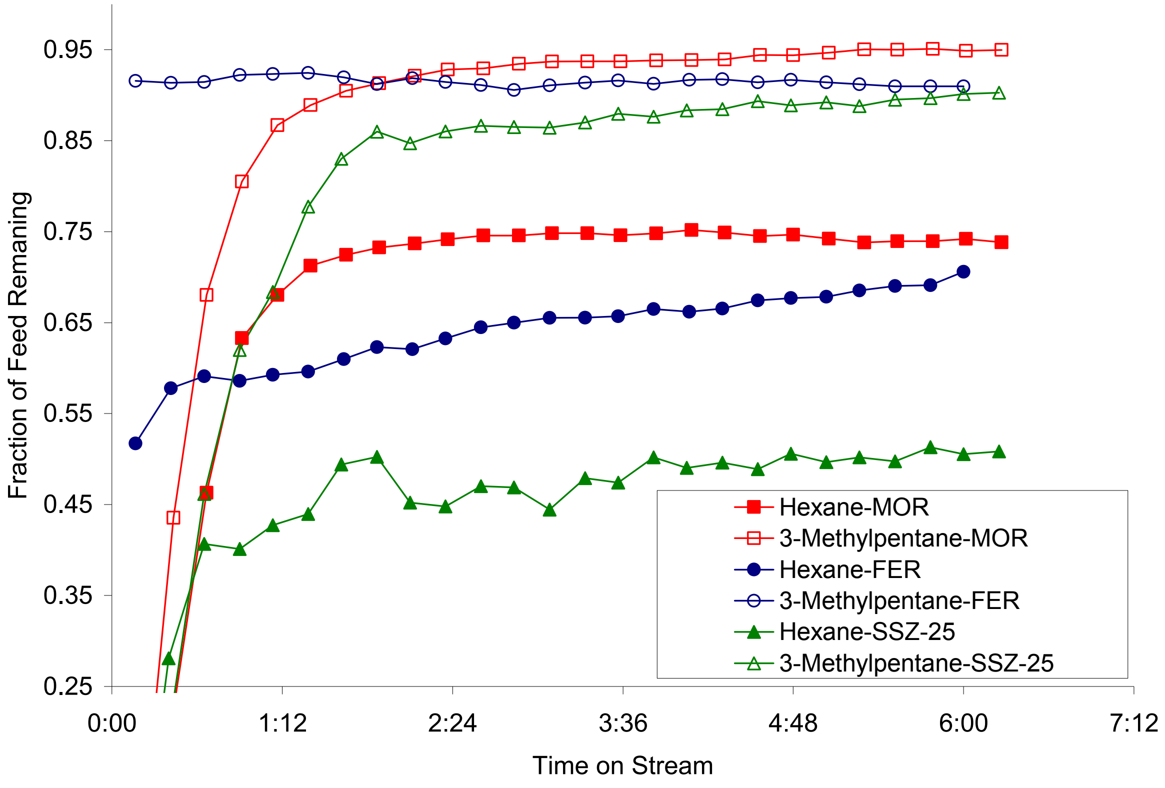

Figure 11.3: Constraint Index testing on partial Na-exchanged MOR and FER.
(As made samples are depicted by blue and partial Na+-exchanged samples by red, solid points = rate of C6 cracking and hollow points = CI.)
Reactions were run using 0.5g zeolite, pelletized and crushed using a 20/40 mesh sieve. The Feed was 5 ml/min (room temp. measurement) of He/Ar and a liquid 50 mol% n-hexane/50 mol% 3-methylpentane feed rate of 10µl/min at 425 °C and atmospheric pressure.

A) MOR

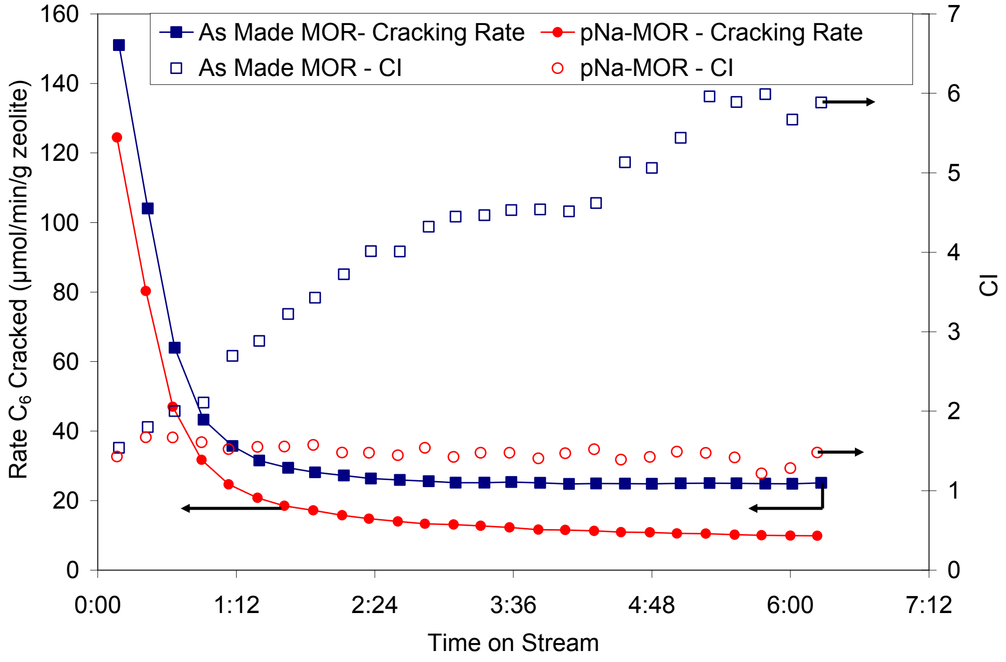

B) FER

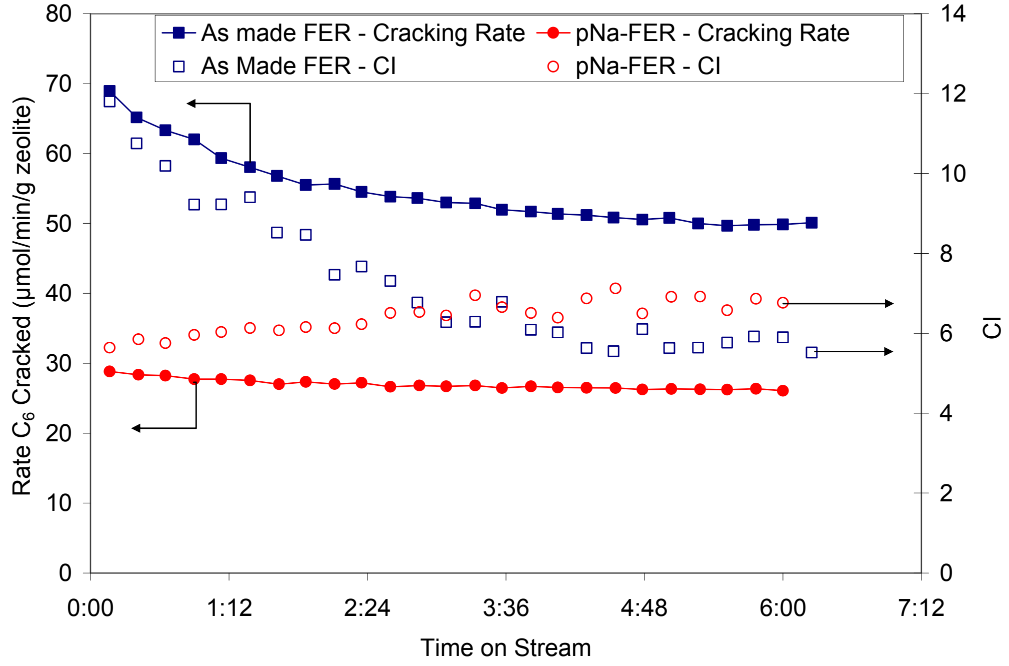

Figure 11.4: Constraint Index test on at 425 °C and 375 °C on ferrierite
Reactions were run using 0.5g zeolite, pelletized and crushed using a 20/40 mesh sieve. The Feed was 5 ml/min (room temp. measurement) of He/Ar and a liquid 50 mol% n-hexane/50 mol% 3-methylpentane feed rate of 10μl/min at atmospheric pressure.

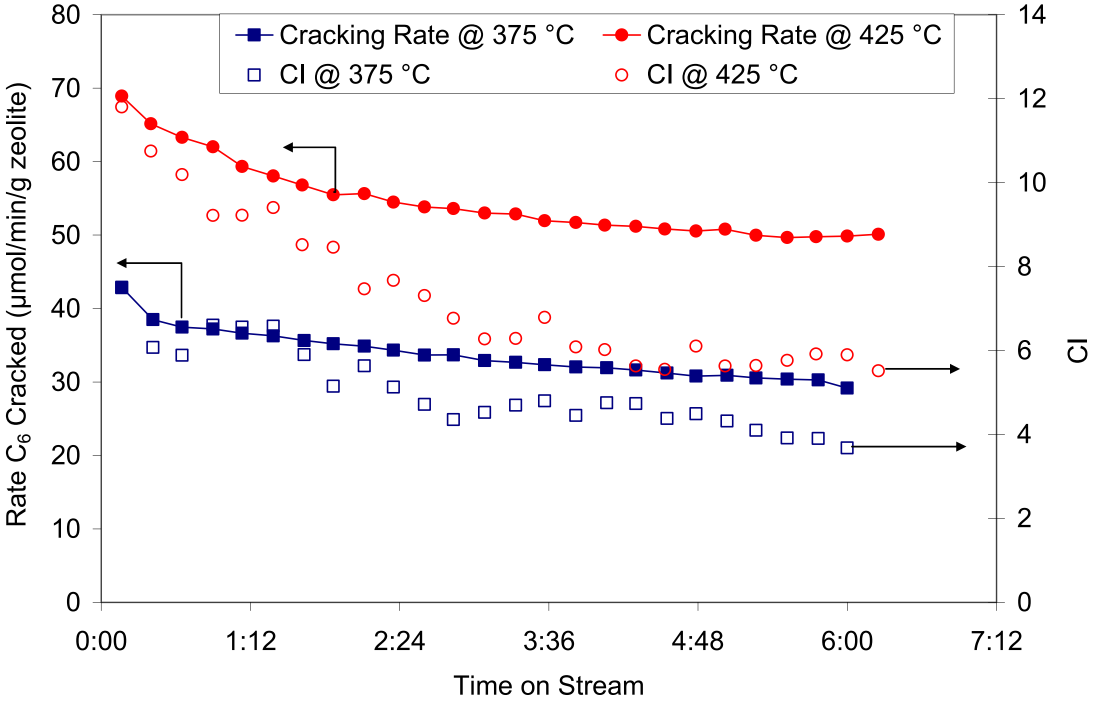

CHAPTER TWELVE

CONCLUSIONS ON STRUCTURE EFFECTS IN CONSTRAINT INDEX TESTING FOR ZEOLITE CHARACTERIZATION

Part Two describes an exploration into the Constraint Index results and possible reasons why the behavior of zeolite structures that contain large cages result in Constraint index values that are typically lower than that expected for the actual pore size of the structure.

The first explanation investigated was that the activity of sites on the external surface may provide a non-selective influence on the cracking reaction and lower the Constraint Index results. The goal was to compare the compare the results on Constraint Index testing on samples of a structure and on the samples of the same structure in which any external surface activity has been removed. ZSM-5 and BEA* were used as a comparison standard of medium and large pore zeolites comparatively and SSZ-35 and SSZ-25 were used as examples of structures with cages. This was accomplished by dealumination by ammonium hexafluorosilicate treatment with the pores of the structure still blocked by the structure directing agent. Little change was noted in the powder X-ray diffraction pattern and scanning electron microscope images of the materials before and after treatment. A small amount of pore blocking was noted by nitrogen adsorption. The Si/Al ratio was seen to predominately be changed at the surface when comparing the surface measurement by x-ray photoelectron spectroscopy analysis or the bulk value measured by inductively coupled plasma optical emission spectroscopy. Samples of ZSM-5, BEA*, and SSZ-35 were then tested for external surface activity by isopropanol dehydration on the samples with and without surface dealumination but before calcinations to keep the pores blocked. External surface activity on all three samples was reduced by over 50 %. After dealumination samples were calcined and tested in the

Constraint Index test. On BEA*, ZSM-5, and SSZ-35 the Constraint Index value was similar between the treated and non-treated samples. SSZ-25 did exhibit a difference in Constraint Index behavior but opposite the changes expected if the external surface was influencing the test.

Hydrocarbon adsorption of n-hexane and 3-methylpentane were performed on several structures; ZSM-5, SSZ-23, SSZ-25, SSZ-28, and SSZ-35 that depict the varying differences in uptake of the individual reactants. However, it is not accurate to assume that these results would translate to reaction conditions. A study of the mass build-up in the materials indicates that the caged structures had a higher propensity for build-up than ZSM-5. It is believed that that this is due to the cages providing more room for transition states need to form the deactivating carbon species as opposed to the channels of ZSM-5.

Finally it was noted that by carrying the Constraint Index out over a longer time period it is possible to discern evidence of multiple distinct features in a structure. In structures such as SSZ-25, MOR, or FER there are either two separate pore structures in the case of SSZ-25 or distinct side pockets off of the larger channels in MOR and FER. In these cases, sites located in the different features foul at different rates. When this happens during the Constraint Index test the Constraint Index value can shift. If the test is only run long enough to determine the first point this information would be lost.

The Constraint Index test is derived from an observed relationship between pore size and the reaction rates of n-hexane and 3-methylpentane cracking, and as such it is not surprising that exceptions to the trend exist. This should always be kept in mind when using the Constraint Index test to characterize a material. A one-point Constraint Index measurement may be misleading and should be used in context with other tests and information. For example, a Constraint Index value similar to ZSM-5 but with much lower activity would suggest a small pore structure with internal cages. Similarly data from adsorption experiments and other reaction-based tests can be used in conjunction to provide a context for characterizing the material. Also further information can be obtained from the behavior of the test over time, which can provide valuable insight.